THE
PHYSICAL
SOCIETY

MEMOIRS

OF THE

COLLEGE OF SCIENCE

KYOTO IMPERIAL UNIVERSITY

SERIES A

VOL. XIV, No. 3

MAY 1931

KYOTO

Mechanical Twins in White Tin and Zinc

By

Kenzo Tanaka and **Keiichi Kamio**

(Received March 20, 1931)

Abstract

A simple method of using Laue-photograph to determine the orientation of twin bands referred to the mother crystal was applied to the case of mechanical twins in white tin and zinc single-crystals and the twinning planes were found to be (331) and ($10\bar{1}2$) respectively.

It is well known that crystals of metals such as zinc, cadmium, bismuth and white tin exhibit twinning when they were subjected to a mecanical stress, and also that the native metal crystals such as gold, silver and copper exhibit banded structures. In the present investigation such circumstances with white tin and zinc were examined by treating the Laue-photograph with the crystallographic globe.[1]

When a Laue-photograph of a crystal containing a twin band is taken, there appear two sets of Laue-spots which belong to the respective parts of the twin. In some cases it is easy to distinguish the Laue-spots belonging to the two parts of the crystal and to determine the relation between their orientation by the size and shape of the spots or, when they are treated by the crystallographic globe, by their mode of arrangement belonging to the same zone of the crystal. In the case of mechanical twins, if we take the Laue-photographs of the crystal before and after the formation of the twin band by the stress, we can easily pick out the Laue-spots due to the twin band.

1. U. Yoshida, Jap. Journ. Phys., **4**, 133 (1927);
S. Takeyama, These Memoirs, **12**, 257 (1929)

Fig. 1, Plate I shows the mechanical twin bands caused by stretching single-crystal plates of white tin, which belongs to the tetragonal lattice type.[1] The initial crystallographic orientations are given in Fig. 1, where the pole of the stereographic projection corresponds to the direction of the normal to the surface of the plate and the vertical direction to the lengthwise direction of it or to that of the stretching. In Fig. 1, Plate I there appear two sets of parallel twin bands in each specimen. Figs. 2 and 3, Plate I are Laue-photographs of two different portions of specimen II each containing

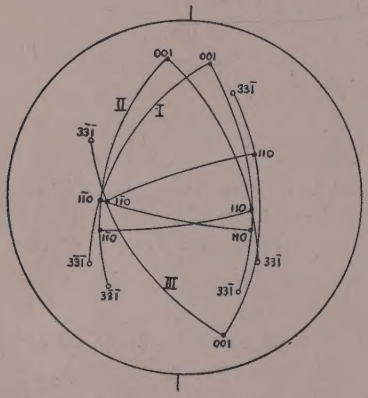

Fig. 1

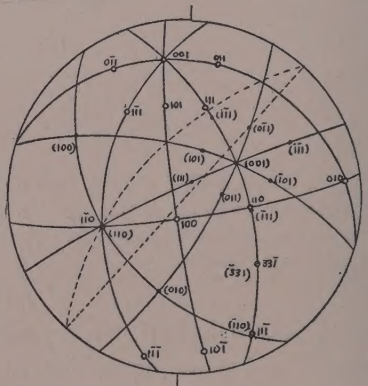

Fig. 2

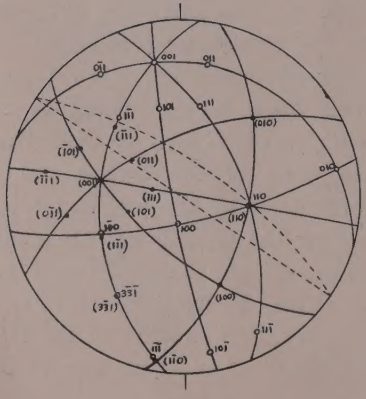

Fig. 3

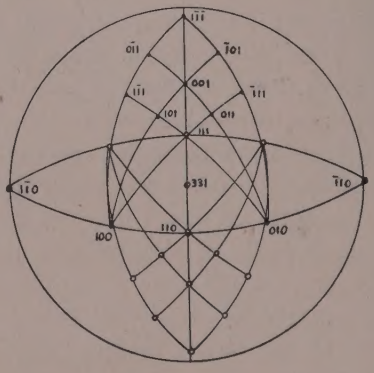

Fig. 4

1. A. E. van Arkel, Proc. Roy. Acad. Amsterdam, **27**, 97 (1924)

a twin band of two different kinds. Both these photographs contain two sets of Laue-spots caused by either of the twin bands and by the mother crystal. The spots that appear in the same positions in both photographs are those due to the mother crystal and the others are those of the twin bands. By treating these two sets of Laue-spots with the crystallographic globe we get the results shown in Figs. 2 and 3, corresponding to Figs. 2 and 3 in Plate I respectively. In these figures the orientation of the crystallographic axes of the mother crystal is shown by small circles and that of twin band by dots whose indices are given in brackets. It is clear from each of these figures that the two components of the twin crystal have a common (331) plane, and with respect to this common plane one component is the mirror image of the other. The orientations of two parallel twin bands on the surface of specimen II are shown by the dotted straight lines respectively in Figs. 2 and 3. These dotted straight lines coincide respectively with the twin planes shown by dotted arcs in the same figures.

The relation between the crystallographic orientations of the component crystals of such twin are shown diagrammatically in Fig. 4 by taking the direction of the twinning axis as the pole. In this figure the position of the crystallographic axes of one component is shown by the dots, and that of the other component is shown by the small circles. The symmetrical distribution of the dots and the small circles in reference to the horizontal diameter of the figure shows that the (331) plane is the twin plane. Other two specimens were also examined in the same way and the same result was obtained. In Fig. 1 the orientations of the crystallographic axes including those of the twin axes are given for the three specimens examined. Of these specimens, the crystallographic orientations are nearly the same and they are roughly symmetrical with respect to the lengthwise direction of the specimen. Crystals having very different orientations from the three above mentioned were also examined, but no twin band was observed to be formed before they were fractured by stretching.

The mechanical twin bands formed in a hexagonal zinc crystal caused by stretching have already been investigated in various ways by many authers,[1] and the twin plane was found to be the $(10\bar{1}2)$ plane. This result was also confirmed by the writers by applying the

1. C. H. Mathewson and A. J. Phillips, Proc. Inst. Met. Div. A. I. M. E., E. Schmid and G. Wasserman, Z. S. f. Phys., **48**, 370 (1928)

method described above. Two Laue-photographs taken with two different twin bands in the same specimen are shown in Figs. 4 and 5, Plate I. In these two photographs the spots marked by small circles are those which are caused by the twin planes of the respective twin bands, and it can be seen that each of them belongs in common to the two sets of Laue-spots of the component crystals. By determining the orientation of the crystals from these photographs it was ascertained that the marked spot was caused by one of the $(10\bar{1}2)$ planes which is common to both components whose orientations are so related that they are mirror images to each other with respect to this plane.

Many specimens composed of large single-crystals of different orientations were tested. Some of the specimens were fractured without showing any twin band, and others showed two or four sets of parallel twin bands on stretching. The results of the examination of such specimens are summarized in Figs. 5, 6 and 7, in which the orientations of the crystals tested are shown by indicating the direction of the normal to the basal plane of the hexagonal zinc crystal by a small circle and the directions of the three normals to the prismatic planes $(10\bar{1}0)$ by dots. The direction of the twin axis or that of the normal to the twin plane $(10\bar{1}2)$ is marked by a small circle with a dot in it, and the direction of the stretching applied to the specimen is taken to be vertical in the figures.

The zinc crystals having the orientations shown in Fig. 5 showed no twin band till they were easily fractured along the basal plane. In the case of Fig. 6 each crystal showed two sets of parallel twin

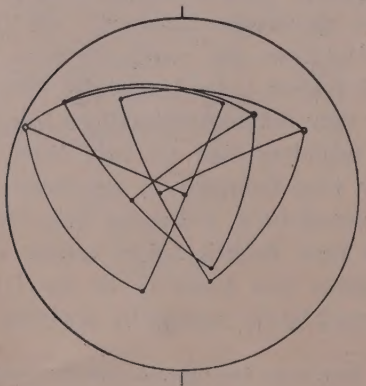

Fig. 5

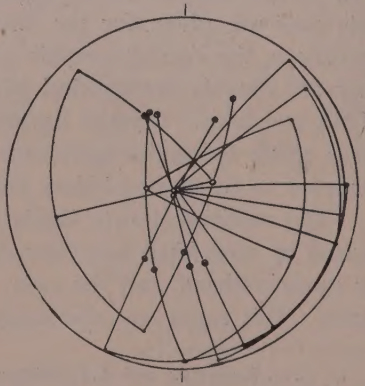

Fig. 6

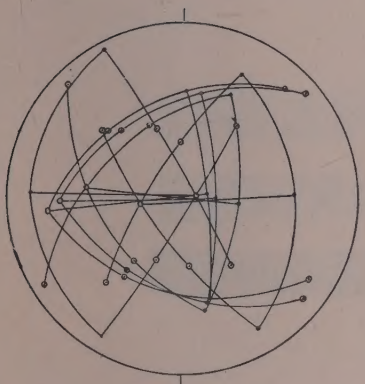

Fig. 7

bands on stretching, and then the crystals were fractured along one of the prismatic $(10\bar{1}0)$ planes belonging to the same zone as the two twin planes and the basal plane. The axis of this zone makes the smallest angle with the plane perpendicular to the direction of stretching, among the similar zones. Fig. 7 shows the orientations of the crystals which formed four sets of parallel twin bands on stretching, and then they were fractured along a prismatic $(10\bar{1}0)$ plane whose normal makes the smallest angle with the direction of stretching or along some irregular zig-zag planes. As may be seen from the figure, these orientations are nearly symmetrical about the lengthwise direction of the specimen and the basal planes make small angles with the direction of stretching.

In conclusion, the writers wish to express their sincere thanks to Prof. U. Yoshida for the interest he has taken in the present research.

Plate I

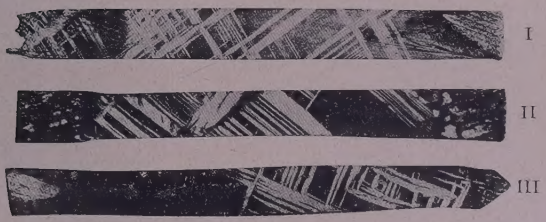

Fig. 1

Fig. 2

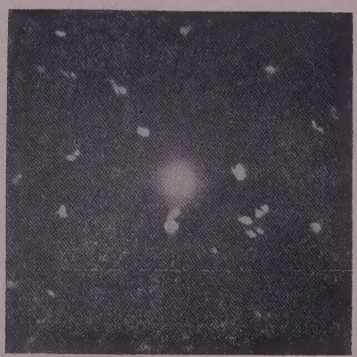

Fig. 3

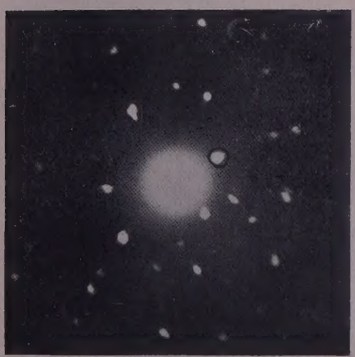

Fig. 4

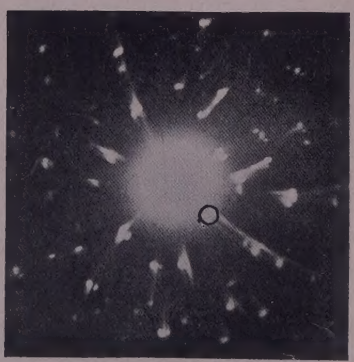

Fig. 5

Sur l'approximation successive et l'unicité de la solution de $\frac{dy}{dx} = f(x, y)$

Par

Hirosi Okamura

(Reçu le 25 mars, 1931)

I. Introduction

Considérons l'équation

$$(1) \qquad \frac{dy}{dx} = f(x, y)$$

et envisageons en particulier la solution qui passe par l'origine $x=0$, $y=0$. Nous admettrons pour le moment que $f(x, y)$ soit continue dans le domaine $D[0 \leqq x \leqq a, \ -b \leqq y \leqq c]$ où $a, b, c > 0$.

Définissons maintenant la fonction $N(x)$ dans l'intervalle $x(0, a)$ comme la borne supérieure (finie ou infinie) de la quantité

$$(2) \qquad \left| \frac{f(x, y) - f(x, \bar{y})}{y - \bar{y}} \right|,$$

quand on fait varier, x étant fixe, l'intervalle non nul $(\bar{y}, y)$ en sorte qu'il occupe toutes les positions contenues dans $(-b, c)$.

Telle fonction $N(x)$ est mesurable B, parce qu'on ne change pas $N(x)$ dans sa définition en se limitant aux seules valeurs rationelles de y et $\bar{y}$ à cause de la continuité de $f(x, y)$, et ainsi $N(x)$ est la borne supérieure d'une infinité dénombrable de fonctions continues de x (2).

Nous proposons, dans ce mémoire, de trouver la condition suffisante pour que l'approximation successive de M. Picard[1] soit con-

1. Traité d'analyse, t. II, 3e éd., p. 368 et suiv.

vergente, au cas plus précis que celui de Lipschitz ou de M. Rosenblatt[1]. Les conditions obtenues sont en même temps les conditions suffisantes pour que la solution soit unique. Pour l'unicité de la solution nous savons déjà plusieurs conditions de la même nature, qui sont plus générales en certains égards. Je veux donner à la fin une simple remarque qui nous a conduit à toutes les conditions.

II. Hypothèses faites sur $f(x, y)$

Nous nous servirons de l'intégrale de Lebesgue au cours des raisonnements suivants, et en outre, ne nous limitant plus à la fonction continue $f(x, y)$, nous adopterons les hypothèses un peu plus larges données par M. Carathéodory[2] sur $f(x, y)$.

Ainsi nous supposerons dans le suivant que

$f(x, y)$ est une fonction finie dans le domaine $D[0 \leqq x \leqq a, -b \leqq y \leqq c]$ $(a, b, c > 0)$, *et, x étant fixe, elle est une fonction continue de y dans l'intervalle $y(-b, c)$ et y étant fixe, elle est une fonction mesurable de x dans l'intervalle $x(0, a)$. De plus elle satisfait à la condition*

$$(3) \qquad |f(x, y)| \leqq M(x),$$

où $M(x)$ est une fonction (finie ou non) sommable dans l'intervalle $x(0, a)$.

C'est évident que la fonction continue répond à ces conditions. D'autre part si l'on constitue la fonction $N(x)$, par la même définition qu'au paragraphe précédent, de la fonction $f(x, y)$ satisfaisant les hypothèses, elle est aussi mesurable. On peut le démontrer tout de suite en remarquant que la fonction (2) est maintenant mesurable au lieu d'être continue au cas précédent. Mais on ne peut plus conclure qu'elle soit mesurable B.

Voici un lemme de M. Carathéodory[3] sur une telle fonction $f(x, y)$.

Si $y(x)$ est une fonction mesurable dans l'intervalle $x(0, a)$ et l'on $a \ -b \leqq y(x) \leqq c$, $f(x, y(x))$ est sommable dans $x(0, a)$.

D'autre part, correspondant à ces nouvelles hypothèses, il suffit de considérer l'équation

$$(4) \qquad y(x) = \int_0^x f(x, y(x))\, dx,$$

1. Arkiv för Math., Astron. och Fys., 5 (1909), 2, p. 1.

2. Vorlesungen über reelle Funktionen, 2e éd., p. 665 et suiv. J'ai fait ici une légère modification.

3. Carathéodory, loc. cit.

au lieu de (1) ; car si $f(x, y)$ est continue, (4) est équivalente à (1).

M. Carathéodory[1] a démontré l'existence de la solution à cette équation générale (4). Mais aux cas particuliers la démonstration par l'approximation successive est aussi possible, comme on le verra d'après ce qui suit.

III. Deux lemmes

Avant d'étudier l'approximation successive, nous donnerons, pour plus de netteté, deux lemmes préliminaires.

Le premier s'énonce comme il suit :

$\varphi'(x)$ et $\nu'(x)$ sont deux fonctions (finies ou non) sommables dans l'intervalle $x(\alpha, \beta)$ $(\alpha<\beta)$, et posons

$$(5) \qquad \nu(x)=\int_\alpha^x \nu'(x)dx+C,$$

C étant arbitraire. D'autre part nous considérons la suite des fonctions, dans le même intervalle

$$(6) \qquad \begin{cases} \varphi(x)=\int_\alpha^x \varphi'(x)dx, \\ \varphi_1(x)=\int_\alpha^x \varphi(x)\nu'(x)dx, \\ \varphi_{n+1}(x)=\int_\alpha^x \varphi_n(x)\nu'(x)dx \qquad (n=1, 2, \ldots\ldots). \end{cases}$$

Alors la série

$$(7) \qquad \varphi(x)+\varphi_1(x)+\varphi_2(x)+\ldots\ldots$$

est toujours convergente dans l'intervalle $x(\alpha, \beta)$, et sa somme est égale à

$$(8) \qquad \varphi(x)+\varphi_1(x)+\varphi_2(x)+\ldots\ldots=e^{\nu(x)}\cdot\int_\alpha^x \varphi'(x)e^{-\nu(x)}dx \qquad (\alpha\leqq x\leqq\beta).$$

Pour le démontrer[2], remarquons d'abord que la fonction $\varphi_n(x)$ est donnée par

$$(9) \qquad \varphi_n(x)=\int_\alpha^x \varphi'(t)\frac{[\nu(x)-\nu(t)]^n}{n!}dt \qquad (n=1, 2, \ldots\ldots).$$

On peut, en effet, le vérifier en différentiant le second membre. Pour

1. Carathéodory, loc. cit.

2. Pour montrer seulement la convergence de (7), on peut procéder un peu plus rapidement. Voir M. Müller, Math. Zeitschr., 26 (1927), p. 627. Mais il paraît ne pas considérer l'intégrale de Lebesgue.

l'effectuer, il faut développer la fonction intégrée par la formule du binôme, faire sortir une puissance de $\nu(x)$ en dehors du signe d'intégration dans chaque terme, et ensuite appliquer la règle de différentiation d'un produit de fonctions. Ainsi on obtient la dérivée du second membre, presque partout,

$$\int_\alpha^x \varphi'(t)dt \,.\, \nu'(x)$$

pour $n=1$, et en général

$$\int_\alpha^x \varphi'(t)\frac{[\nu(x)-\nu(t)]^{n-1}}{(n-1)!}dt \,.\, \nu'(x) \qquad (n=2, 3, \ldots\ldots).$$

On voit d'autre part la continuité absolue du second membre de (9) par le développement indiqué, car la somme et le produit des fonctions absolument continues le sont aussi. Par conséquent la relation (9) s'établit successivement.

Or considérons la série

$$\varphi'(t)+\varphi'(t)\frac{\nu(x)-\nu(t)}{1!}+\varphi'(t)\frac{[\nu(x)-\nu(t)]^2}{2!}+\ldots\ldots,$$

x étant regardé comme paramètre arbitraire dans $x(\alpha,\beta)$. Cette série converge presque partout (sauf les points où $\varphi'(t)$ devient infinie) vers $\varphi'(t)e^{\nu(x)-\nu(t)}$, et la somme de quelques premiers termes ne surpasse jamais en valeur absolue la fonction sommable $|\varphi'(t)|e^{|\nu(x)-\nu(t)|}$. Donc, par le théorème de M. Lebesgue[1], nous avons

$$\int_\alpha^x \varphi'(t)dt+\int_\alpha^x \varphi'(t)\frac{[\nu(x)-\nu(t)]}{1!}dt+\int_\alpha^x \varphi'(t)\frac{[\nu(x)-\nu(t)]^2}{2!}dt$$
$$+\ldots\ldots=\int_\alpha^x \varphi'(t)e^{\nu(x)-\nu(t)}dt \qquad (\alpha\leqq x\leqq\beta).$$

C'est la relation demandée (8), en vertu de (9). (C. q. f. d.)

Passons maintenant au second lemme.

Cette fois supposons que les fonctions $\varphi'(x)$ *et* $\nu'(x)$ *ne soient pas négatives,* $\varphi'(x)$ *sommable dans* $x(\alpha, \beta)$ *comme précédemment, mais* $\nu'(x)$ *ne sommable que dans l'intervalle* $(\alpha+\eta, \beta)$, *quel que soit le nombre positif* η. *Soit donc au lieu de* (5)

$$\nu(x)=\int_\delta^x \nu'(x)dx+C,$$

1. De la Vallée Poussin, Intégrale de Lebesgue, etc., p. 49.

δ étant un nombre tel que $\alpha<\delta\leqq\beta$.

Alors pour qu'on puisse former les fonctions

$$\varphi_1(x),\ \varphi_2(x),\ \ldots\ldots$$

successivement par les formules (6), *c'est-à-dire que les fonctions*

$$\varphi(x)\nu'(x),\ \varphi_1(x)\nu'(x),\ \ldots\ldots$$

soient toutes sommables dans $x(\alpha,\ \beta)$, *et de plus la série*

$$\varphi(x)+\varphi_1(x)+\varphi_2(x)+\ldots\ldots \tag{10}$$

formée de ces fonctions soit convergente dans $x(\alpha,\ \beta)$, *il faut et il suffit que*

$$\varphi'(x)e^{-\nu(x)}$$

soit sommable dans $x(\alpha,\ \beta)$.

Quand ces conditions sont remplies, nous avons aussi

$$\varphi(x)+\varphi_1(x)+\varphi_2(x)+\ldots\ldots=e^{\nu(x)}\cdot\int_\alpha^x\varphi'(x)e^{-\nu(x)}dx\quad(\alpha\leqq x\leqq\beta). \tag{11}$$

Nous prouverons ce lemme comme il suit :

Définissons, pour chaque valeur d'un paramètre $\gamma(\alpha<\gamma\leqq\beta)$, les fonctions $\Phi(x,\ \gamma)$, $\Phi_1(x,\gamma)$, $\Phi_2(x,\gamma)$, ... dans l'intervalle $x(\alpha,\beta)$ de façon qu'elles s'annulent toutes dans $x(\alpha,\gamma)$ et soient assujetties dans $x(\gamma,\beta)$ aux conditions suivantes analogues à (6)

$$\begin{cases}\Phi(x,\ \gamma)=\int_\gamma^x\varphi'(x)dx,\\ \Phi_1(x,\gamma)=\int_\gamma^x\Phi(x,\gamma)\nu'(x)dx=\int_\alpha^x\Phi(x,\gamma)\nu'(x)dx,\\ \Phi_{n+1}(x,\gamma)=\int_\gamma^x\Phi_n(x,\gamma)\nu'(x)dx=\int_\alpha^x\Phi_n(x,\gamma)\nu'(x)dx\ \ (n=1,2,\ldots).\end{cases} \tag{12}$$

Ces fonctions sont toutes non négatives, et quand on fait tendre γ à α, elles vont constamment en croissant à chaque point de $x(\alpha,\beta)$.

D'abord on a évidemment

$$\lim_{\gamma\to\alpha}\Phi(x,\gamma)=\varphi(x)\qquad(\alpha\leqq x\leqq\beta).$$

Donc $\Phi(x,\gamma)\nu'(x)$ tend en croissant vers $\varphi(x)\nu'(x)$ lorsque γ se rapproche de α. Par conséquent en appliquant le théorème donné par M. de la Vallée Poussin[1] on arrive aux résultats suivants.

---

1. De la Vallée Poussin, loc. cit., p. 49.

Si $\varphi_1(x)$ existe c'est-à-dire si $\varphi(x)\nu'(x)$ est sommable dans $x(\alpha, \beta)$, on a

$$\lim_{\gamma\to\alpha}\int_\alpha^x \Phi(x,\gamma)\nu'(x)dx=\int_\alpha^x \varphi(x)\nu'(x)dx \qquad (\alpha\leqq x\leqq\beta),$$

ou, par (12),

$$\lim_{\gamma\to\alpha} \Phi_1(x,\gamma)=\varphi_1(x) \qquad (\alpha\leqq x\leqq\beta).$$

Au contraire si $\varphi(x)\nu'(x)$ n'est pas sommable dans $x(\alpha, \beta)$, il en est ainsi au voisinage arbitraire de α et l'on a

$$\lim_{\gamma\to\alpha}\int_\alpha^x \Phi(x,\gamma)\nu'(x)dx=+\infty \qquad (\alpha< x\leqq\beta),$$

ou, par (12),

$$\lim_{\gamma\to\alpha} \Phi_1(x,\gamma)=+\infty \qquad (\alpha< x\leqq\beta).$$

Nous avons expliqué ici sur $\Phi_1(x,\gamma)$ et $\varphi_1(x)$, mais quand $\varphi_1(x)$ existe c'est la même chose pour $\Phi_2(x,\gamma)$ et $\varphi_2(x)$, et ainsi de suite successivement.

Donc, en somme, quand $\varphi(x)$, $\varphi_1(x)$, $\varphi_2(x)$, ...toutes existent, pour n arbitraire, on a

$$\lim_{\gamma\to\alpha} \Phi_n(x,\gamma)=\varphi_n(x) \qquad (\alpha\leqq x\leqq\beta). \tag{13}$$

Mais quand $\varphi(x)$, $\varphi_1(x)$, ..., $\varphi_{i-1}(x)$ seules existent, et $\varphi_i(x)$ n'existe plus, (13) est vraie pour $n\leqq i-1$, et

$$\lim_{\gamma\to\alpha} \Phi_i(x,\gamma)=+\infty \qquad (\alpha< x\leqq\beta). \tag{14}$$

D'autre part, en vertu du premier lemme, on sait

$$\Phi(x,\gamma)+\Phi_1(x,\gamma)+\Phi_2(x,\gamma)+.....=e^{\nu(x)}\cdot\int_\gamma^x \varphi'(x)e^{-\nu(x)}dx. \tag{15}$$

Dans le premier membre chaque terme n'est pas négatif et il ne décroît pas quand on fait tendre γ à α. A cause de (13) et (14) la limite de ce premier membre est finie, si et seulement si la série (10) est convergente. Dans ce cas la limite est la somme de (10). Ainsi l'égalité (15) devient (11) par le passage à la limite. (C. q. f. d.)

IV. Approximation successive

Revenons à (4).

Prenons une fonction $y_0(x)$, mesurable dans $x(0, a')$ $(0< a'\leqq a)$ et bornée entre $-b$ et c, d'ailleurs arbitraire. Choisissant a' convenablement, on peut former les fonctions

(16) $\qquad y_0(x), y_1(x), y_2(x), \ldots\ldots$

successivement par les formules

(17) $\qquad y_{n+1}(x)=\int_0^x f(x, y_n(x))dx \qquad (n=0, 1, 2, \ldots\ldots),$

ceci étant possible en vertu du lemme de II. Il suffit de prendre a' tel que

$$\begin{cases} 0<a'\leqq a, \\ \int_0^{a'} M(x)dx\leqq b, c. \end{cases}$$

Quelquefois on peut prendre a' plus grand, mais nous n'insisterons pas sur cette question.

Lorsque la suite (16) converge dans $x(0, a')$, sa limite $Y(x)$ satisfait à l'équation (4)[1]. C'est la conséquence du passage à la limite de (17). Le premier membre tend manifestement vers $Y(x)$, et le second membre, à cause de (3) et de la continuité de $f(x, y)$ par rapport à y, a pour limite

$$\int_0^x f(x, Y(x))dx,$$

par le théorème de M. Lebesgue.

Cette suite des fonctions (16) converge si $N(x)$ est sommable dans $x(0, a)$. Elle converge aussi lorsqu'au moins, $N(x)$ est sommable dans $x(\eta, a)$ pour tout nombre positif η et si les conditions suivantes sont remplies.

Pour certain nombre entier positif (ou nul) j, on a

(18) $\qquad |y_{j+1}(x)-y_j(x)|\leqq\int_0^x \psi'(x)dx \qquad (0\leqq x\leqq a'),$

où $\psi'(x)$ est une fonction non négative sommable dans $x(0, a')$ en même temps que la fonction $\psi'(x)e^{-L(x)}$ où $L(x)$ est, par définition,

(19) $\qquad L(x)=\int_\delta^x N(x)dx \qquad (0<\delta\leqq a').$

De plus, au cas où ces conditions sont remplies, on a sur la limite $Y(x)$ de (16) la formule

(20) $\qquad |Y(x)-y_j(x)|\leqq e^{L(x)}\cdot\int_0^x \psi'(x)e^{-L(x)}dx \qquad (0\leqq x\leqq a'),$

et $Y(x)$ satisfait à l'équation (4) dans $x(0, a')$.

---

1. Le raisonnement d'ici se trouve déjà dans le mémoire de M. Nikliborc, Studia Mathematica, 1 (1929), p. 203. Voir aussi le mémoire cité de M. Müller, p. 621.

La vérité de ces résultats est la conséquence immédiate des lemmes du paragraphe précédent. Faisons correspondre en effet $\psi'(x)$, $N(x)$ et $L(x)$ aux $\varphi'(x)$, $\nu'(x)$ et $\nu(x)$ des lemmes et définissons les fonctions $\psi(x)$, $\psi_1(x)$, $\psi_2(x)$, ...pareillement aux $\varphi(x)$, $\varphi_1(x)$, $\varphi_2(x)$, ...

Alors il résulte de (17) et (18) successivement

$$|y_{j+n+1}(x)-y_{j+n}(x)| \leqq \psi_n(x) \qquad (n=0, 1, 2, \ldots\ldots),$$

et, par conséquent, la série

$$(y_{j+1}(x)-y_j(x))+(y_{j+2}(x)-y_{j+1}(x))+\ldots\ldots$$

est majorée par la série convergente

$$\psi(x)+\psi_1(x)+\psi_2(x)+\ldots\ldots = e^{L(x)}\cdot\int_0^x \psi'(x)e^{-L(x)}dx,$$

d'où l'on conclut la convergence de (16) et la formule (20).

Il faut remarquer deux cas simples où la suite (16) remplit ces conditions quelle que soit la fonction de départ $y_0(x)$. Ce sont les cas :

1° *où* $N(x)$ *est sommable dans* $x(0, a)$;

2° *où, plus généralement,* $N(x)$ *est sommable dans* $x(\eta, a)$ *pour tout nombre positif* η *et la fonction* $M(x)e^{-L(x)}$ *est sommable dans* $x(0, a)$.

Dans ces cas la condition de convergence (18) est satisfaite, comme on le voit par

$$|y_2(x)-y_1(x)| \leqq \int_0^x |f(x, y_1(x))-f(x, y_0(x))|\,dx \leqq \int_0^x 2M(x)dx.$$

Enfin dans ces deux cas la solution de (4) est unique. Car si $y(x)$ est une solution quelconque, on a

$$|y(x)-y_1(x)| \leqq \int_0^x |f(x, y(x))-f(x, y_0(x))|\,dx \leqq \int_0^x 2M(x)dx,$$

et regardant $2M(x)$ et $N(x)$ comme $\varphi'(x)$ et $\nu'(x)$ des lemmes du paragraphe précédent, on a successivement

$$\begin{aligned}|y(x)-y_{n+1}(x)| &\leqq \int_0^x |f(x, y(x))-f(x, y_n(x))|\,dx \\ &\leqq \int_0^x |y(x)-y_n(x)|\,N(x)dx \leqq \int_0^x \varphi_{n-1}(x)N(x)dx = \varphi_n(x).\end{aligned}$$

Or $\varphi_n(x)$ tend vers zéro par les lemmes et

$$\lim_{n\to\infty} |y(x)-y_{n+1}(x)| = |y(x)-Y(x)| = 0.$$

Donc

$$y(x) = Y(x).$$

On verra une autre démonstration de l'unicité de la solution dans VI.

M. Carathéodory[1] a appelé la *condition de Lipschitz* celle du cas 1°, et il a donné une démonstration de l'unicité de la solution.

Le cas 2° comprend comme cas particulier celui où $f(x, y)$ est bornée et $e^{-K(x)}$ est sommable. La sommabilité est satisfaite si

$$N(x) \leqq \frac{k}{x} \qquad (0 < k < 1).$$

C'est la condition de M. Rosenblatt.

V. Exemples

Comme exemple, considérons l'équation

$$\frac{dy}{dx} = \sqrt{|y| + [\omega(x)]^2},$$

où $\omega(x)$ est une fonction continue s'annulant une infinité de fois au voisinage de 0, mais son inverse $\frac{1}{\omega(x)}$ étant sommable. Dans ce cas on a évidemment

$$N(x) = \frac{1}{2|\omega(x)|}.$$

Donc cet exemple appartient au cas 1° du paragraphe précédent. Pour la fonction $\omega(x)$, posons, par exemple,

$$\omega(x) = \left(x \sin \frac{1}{x}\right)^{\frac{1}{3}}.$$

La sommabilité de $\frac{1}{\omega(x)}$ vient de la convergence de la série

$$\sum_{n=1}^{\infty} \int_{\frac{1}{(n+1)\pi}}^{\frac{1}{n\pi}} \frac{dx}{\left| x \sin \frac{1}{x} \right|^{\frac{1}{3}}}.$$

C'est facile à voir si l'on change le variable

$$\int_{\frac{1}{(n+1)\pi}}^{\frac{1}{n\pi}} \frac{dx}{\left| x \sin \frac{1}{x} \right|^{\frac{1}{3}}} = \int_0^{\pi} \frac{d\xi}{(\xi + n\pi)^{\frac{5}{3}} (\sin \xi)^{\frac{1}{3}}}, \quad \left(\frac{1}{x} = \xi + n\pi\right)$$

$$\leqq \frac{1}{(n\pi)^{\frac{5}{3}}} \int_0^{\pi} \frac{d\xi}{(\sin \xi)^{\frac{1}{3}}}.$$

1. Carathéodory, loc. cit.

Autrefois M. Nagumo[1] a étudié le cas critique

$$N(x) \leqq \frac{1}{x},$$

qui ne rentre pas dans le cas 2°. Dans ce cas il peut arriver qu'une infinité de solutions satisfassent à l'équation (4), comme on le voit par le simple exemple suivant,

$$f(x,y) = \begin{cases} 0 & (x=0), \\ 1 & \left(x \neq 0,\ \frac{y}{x} > 1\right), \\ \frac{y}{x} & \left(x \neq 0,\ \left|\frac{y}{x}\right| \leqq 1\right), \\ -1 & \left(x \neq 0,\ \frac{y}{x} < -1\right). \end{cases}$$

$f(x,y)$ satisfait aux conditions de II pour un domaine convenable D, quoique (4) ait une infinité de solutions

$$y = cx, \qquad |c| \leqq 1.$$

Cet exemple nous montre que le théorème de M. Nagumo n'est pas vrai sous les seules conditions de II, et il nous faut une autre condition que nous étudierons dans le paragraphe suivant.

VI. Remarque sur les conditions d'unicité

Bornons-nous au cas où $N(x)$ ou plus généralement $N_1(x)$ est sommable au moins dans $x(\eta, a)$, si petit qu'il soit le nombre positif η. $N_1(x)$ est définie tout à fait pareillement à $N(x)$, excepté que l'on prend au lieu de (2)

$$\frac{f(x,y) - f(x,\bar{y})}{y - \bar{y}}, \tag{21}$$

pas la valeur absolue. Comme $N(x)$, $N_1(x)$ est mesurable, et manifestement on a

$$|N_1(x)| \leqq N(x), \tag{22}$$

$N_1(x)$ pouvant être négative.

En effet, supposons qu'on ait deux solutions distinctes $y(x)$ et $\bar{y}(x)$ de l'équation (4) au voisinage de $x=0$. Il est admissible de supposer qu'une d'elles ne soit jamais inférieure à l'autre. Pour l'assurer

1. Japanese Jour. Math., 3 (1926), p. 107, et 4 (1927), p. 307.

il suffit de décomposer l'intervalle d'intégration (o, x) du second membre de (4) à l'ensemble fermé E où l'on a $y(x)=\bar{y}(x)$ et aux intervalles contigus à E. Ainsi nous savons que la fonction prenant à chaque point la valeur plus grande ou plus petite de $y(x)$ et $\bar{y}(x)$ satisfait à (4). Donc nous admettrons toujours

$$y(x)\geqq\bar{y}(x).$$

Alors nous avons deux relations fondamentales

$$(23)\qquad y(x)-\bar{y}(x)=\int_o^x[f(x,y(x))-f(x,\bar{y}(x))]dx,$$

et, presque partout (sauf les points où $N_1(x)=+\infty$),

$$(24)\qquad f(x,y(x))-f(x,\bar{y}(x))\leqq N_1(x)\ [y(x)-\bar{y}(x)].$$

Posons, pour simplifier l'écriture,

$$(25)\qquad \begin{cases}\chi(x)=y(x)-\bar{y}(x)=\int_o^x[f(x,y(x))-f(x,\bar{y}(x))]dx,\\ \chi'(x)=f(x,y(x))-f(x,\bar{y}(x)).\end{cases}$$

En combinant (23) et (24)[1] avec les notations de (25), on a

$$\chi'(x)\leqq N_1(x)\chi(x)$$

ou

$$e^{-L_1(x)}.[\chi'(x)-N_1(x)\chi(x)]\leqq o,$$

où, par définition,

$$L_1(x)=\int_\delta^x N_1(x)dx\qquad (o<\delta\leqq a).$$

Donc la fonction absolument continue et non négative de $x(x>o)$

$$e^{-L_1(x)}.\chi(x)$$

ne croît jamais, et l'on a ensuite

$$(26)\qquad \lim_{x\to 0} e^{-L_1(x)}.\chi(x)>o.$$

Cette inégalité joue un rôle essentiel. Nous en déduirons plusieurs conditions suffisantes pour que la solution de (4) soit unique. Nous les démontrons par l'absurde en montrant sous quelques hypothèses que

$$(27)\qquad \lim_{x\to 0} e^{-L_1(x)}.\chi(x)=o.$$

D'abord si $f(x,y)$ est continue à l'origine, c'est-à-dire si

$$(28)\qquad \lim_{\substack{x\to 0\\ y\to 0}} f(x,y)=f(o,o),$$

1. Ce mode de combinaison est nouveau, à notre connaissance.

en vertu du théorème de la moyenne appliqué sur

$$\int_0^x [f(x, y(x)) - f(x, \bar{y}(x))]dx,$$

on aura la condition

$$(29) \qquad e^{-L_1(x)} \cdot x < P,$$

P étant une constante, d'où l'on conclut (27).

M. Fukuhara[1] a déjà trouvé la condition de cette forme au cas plus restreint.

Cette condition (29) contient comme cas particuliers les conditions

$$N(x) \leqq \frac{1}{x}$$

de M. Nagumo et

$$N(x) \leqq \frac{1+\varepsilon(x)}{x}$$

de M. Shimizu[2], où $\varepsilon(x)$ $(x>0)$ est continue et positive, $\frac{\varepsilon(x)}{x}$ étant intégrable dans $x(0, a)$.

Au lieu de la continuité (28) si nous savons seulement que

$$\lim_{\substack{x\to 0 \\ y\to 0}} x^p f(x, y) = 0 \qquad (0<p<1),$$

il nous suffit pour conclure (27), ou bien

$$e^{-L_1(x)} \cdot x^{1-p} < P_1,$$

P_1 étant une constante, ou bien la condition plus forte

$$N(x) \leqq (1-p)\frac{1+\varepsilon(x)}{x},$$

$\varepsilon(x)$ ayant le même sens. C'est la condition de M. Watanabe[3].

Enfin pour conclure (27) il suffit aussi

$$\lim_{x\to 0} e^{-L_1(x)} \cdot \int_0^x M(x)dx = 0.$$

Ceci implique le cas où $e^{-L(x)} \cdot M(x)$ est sommable, la condition 2° du paragraphe IV, parce que, $e^{-L(x)}$ étant non croissant, on a au voisinage de $x=0$

$$\int_0^x e^{-L(x)} \cdot M(x)dx \leqq e^{-L(x)} \cdot \int_0^x M(x)dx \leqq e^{-L_1(x)} \cdot \int_0^x M(x)dx.$$

1. Japanese Jour. Math., 5 (1928), p. 246.
2. Proc. Imp. Acad., 4 (1928), p. 328.
3. Japanese Jour. Math., 7 (1930), p. 209.

The Arrangement of the Micro-Crystals in Compressed Single-Crystal-Plates of Aluminium, Part III

By

Yoshio Fukami

(Received March 27, 1931)

Abstract

When a rectangular single crystal plate of aluminium was compressed to a thickness of 3 %–10 % of the initial thickness, the axis of the imperfect fibrous arrangement of the micro-crystals, owing to the destruction of the single crystal by compression, was always parallel to the direction of the flow of the metal by compression. It was found that according to the initial orientation of the crystallographic axes with reference to the specimen and the direction of the flow of the metal by compression, such fibrous arrangement could be classified into four types:— (1) The [110] axis was nearly parallel to the longer side of the specimen, the fibrous axis [111] was parallel to the direction of the flow of the metal by compression, and thus the (211) plane was nearly parallel to the flat surface of the specimen. (2) The [111] axis was nearly parallel to the longer side, the fibrous axis [211] was parallel to the direction of the flow of the metal, and thus the (110) plane was nearly parallel to the flat surface. (3) The [110] axis was parallel to the longer side, the fibrous axis [100] was parallel to the direction of the flow of the metal, and thus the [110] plane was nearly parallel to the flat surface. (4) The [100] axis was parallel to the longer side, the fibrous axis [110] was parallel to the direction of the flow of the metal, and thus the (110) plane was parallel to the flat surface. Of the four types of the fibrous arrangement mentioned above, the first two occured more frequently than the last two. The relation between the fibrous arrangement of the micro-crystals in a rectangular plate which is caused by compression of such high degree and of the micro-crystals in rolled aluminium foils was also examined both for single- and polycrystalline specimens, and it became clear that the fibrous arrangement of the micro-crystal was almost the same in both cases, if we regard the direction of the flow of metal on compression as the direction of rolling.

In the two previous investigations[1], the writer examined the arrangement of the micro-crystals in compressed circular and rectangular single crystal plates of aluminium. The micro-crystals in a circular

1. These Memoirs, **12**, 261 (1929);— **13**, 299 (1930)

plate rotated themselves, on compression, in such a manner that the (110) plane which made the slightest inclination to the flat surface of the plate became nearly parallel to the flat surface of the specimen on making the [111] or [110] axis which was almost parallel to the flat surface the axis of rotation of the micro-crystals by compression; and when the specimen was compressed to a thickness of less than 30% of the initial thickness, the [110] axis which was nearly perpendicular to the flat surface became the axis of rotation of the micro-crystals. The micro-crystals in a rectangular plate rotated themselves in such a manner that the (110) plane, which made the slightest inclination to the flat surface, became nearly parallel to the flat surface of the specimen, the [111], [110] or [211] axis which was almost parallel to the longer side of the specimen being taken as the axis of rotation of the micro-crystals. It was also stated in the former papers that in the case of circular plates, the (110) plane which was nearly parallel to the flat surface of the specimen was able to become completely parallel to the flat surface on compression, but in rectangular plates it happened sometimes that the (110) plane which was nearly parallel to the flat surface of the specimen was not able to become completely parallel to the flat surface according to the initial crystallographic orientation, being restricted by the condition that the direction of the fibrous axis [111], [110] or [211] axis remained unchanged by compression. In the previous experiments with rectangular plates the specimen were compressed to the thickness of 25%–95% of the initial thickness. In the present investigation, the single crystal specimens of aluminium in the form of rectangular plates were still compressed to the thickness of 3%–10% of the initial thickness. The machine which was used to compress the specimen was a hydraulic press with a maximum pressure of $30{,}000^{kgms}$. With this hydraulic press it was difficult to compress the specimen to a thickness of less than 3% of the initial thickness. The size of the single crystal plate which was obtained by the stress-annealing method was generally 3 cms. × 1cm. × 1mm. A rectangular plate whose longer side was about five times longer than the shorter side was obtained from the specimen above mentioned by etching off slowly its outer portion with some dilute acid. When the single crystal specimens thus prepared were compressed to less than 10% of the initial thickness, the axis of the fibrous arrangement of the micro-crystals of aluminium became always parallel at last to the direction of the flow of the metal caused by the compression; and it was found that such a final state of the fibrous

arrangement might be classified into the following four types:— (1) The fibrous axis [111] axis was parallel to the direction of the flow of the metal, the [110] axis was nearly parallel to the longer side of the specimen and consequently the (211) plane was nearly parallel to the flat surface of the specimen. (2) The [211] axis was parallel to the direction of the flow of the metal, the [111] axis was nearly parallel to the longer side, and consequently the (110) plane was nearly parallel to the flat surface. (3) The [100] axis was parallel to the direction of the flow of the metal, the [110] axis was nearly parallel to the direction of the longer side, and consequently the (110) plane was nearly parallel to the flat surface. (4) The [110] axis was parallel to the direction of the flow of the metal, the [100] axis was nearly parallel to the longer side, and consequently the (110) plane was nearly parallel to the flat surface. In the following four sections the details of the results obtained in the experiments are described.

Fig. 1

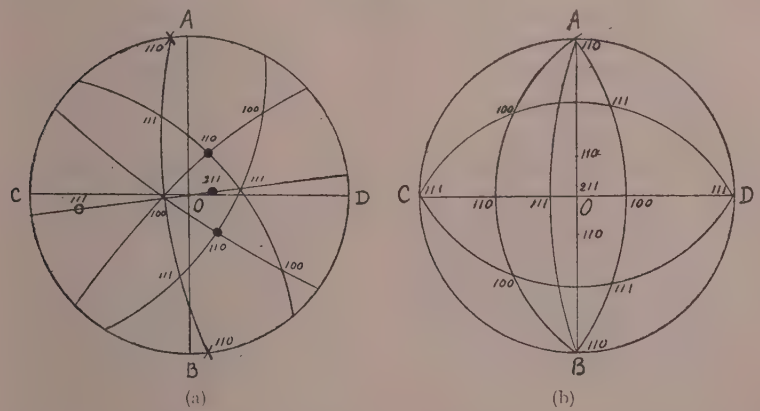

(I) The [111] axis is parallel to the direction of the flow of the metal on compression, the [110] axis is nearly parallel to the longer side of the specimen, and consequently the (211) plane is parallel to the flat surface of the specimen.

(a) of Fig. 1 represents the initial crystallographic orientation of a single crystal specimen whose thickness was 0.85 mm. The line AB is the direction of the longer side of the specimen and the line CD is the direction of the flow of the metal on compression. As stated in the description of the previous experiment, when such a

specimen was compressed little by little, the [110] axis shown by a cross became the axis of rotation of the micro-crystals produced by the compression, and the two [110] axes shown by the dots approached gradually to the line AB. Consequently the [111] axis shown by a small circle became gradually parallel to the direction of the flow of the metal on compression. As the direction of the [110] axis shown by a cross remained almost unchanged during the whole process of compression, the [110] axes shown by the dots were not able to come completely to the centre O. In other words the (110) plane which made the slightest inclination to the flat surface of the specimen was not able to become completely parallel to the flat surface. Fig. 1 of Plate I is a Laue-photograph taken with the specimen which was compressed to a thickness of 3% of the initial thickness, by sending the X-ray beam from a molybdenum target normally to the flat surface of the specimen. It is found from this photograph that the [110] axis is nearly parallel to the longer side of the specimen and the [111] axis is nearly parallel to the direction of the flow of the mental on compression, and consequently that the (211) plane is nearly parallel to the flat surface of the specimen. The ideal orientation of the micro-crystals in the specimen is thus just as shown by (b) in Fig. 1, when the specimen is compressed to a thickness of 3% of the initial thickness. Next the writer examined the angle of deviation of the crystallographic axes of the micro-crystals in the specimen from those of the ideal orientation. The amount of the angle of such deviation of the crystallographic axes of the micro-crystals was estimated from the elongation of the Laue-spots which were caused by a small scattering of the crystallographic orientation of the micro-crystals, near their ideal orientation. From the photograph reproduced in Fig. 1 of Plate I, the maximum deviation of the [111] axis, which is nearly in the direction of the flow of the metal, from the flat surface of the specimen is thus found to be about $\pm 14^\circ$; and the maximum deviation of the [110] axis, which is nearly in the direction parallel to the longer side, from the flat surface is found to be about $\pm 21^\circ$. Consequently the maximum deviation of the (211) plane which is nearly parallel to the flat surface is $\pm 14^\circ$ in the direction of the flow of the metal, and $\pm 21^\circ$ in the direction parallel to the longer side of the specimen. That is to say, the deviation of the crystallographic orientation of the micro-crystals is less in the direction of the flow of the metal than in the direction parallel to the longer side of the specimen for compression of such high degree. Judging from this, it seems natural to say

that the fibrous axis of the micro-crystals for slight compression is parallel to the direction of the longer side of the specimen and remains almost unchanged till the specimen is compressed to about 25% of the initial thickness, as reported in the former reports; but the fibrous axis changes for compression less than 10% of the initial thickness and finally becomes parallel to the direction of the flow of the metal. The above stated facts were also ascertained diagrammatically. The writer assumed that the [111] axis is the axis of the fibrous arrangement, in the direction of the flow of the metal on compression, the [110] axis is nearly in the direction of the longer side of the specimen, that the maximum deviation of the [111] axis from the flat surface is $\pm 14^\circ$ and the maximum deviation of the [110] axis from the flat surface, $\pm 21^\circ$. On these assumptions, the diffraction diagram of the X-rays that might be expected to be impressed on the photographic plates by the K_α-line of molybdenum impinging normally to the flat surface of the specimen was drawn. Fig. 2 shows the diagram thus calculated and a fair agreement between this diagram and the photograph

Fig. 2

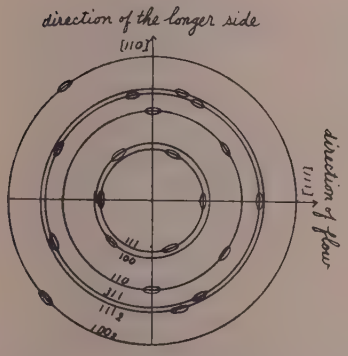

Fig. 3

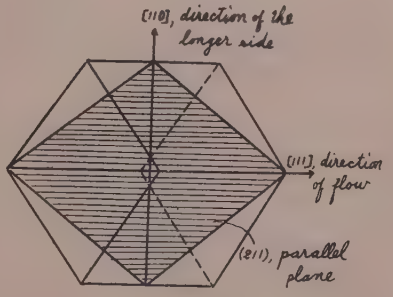

shown in Fig. 1 of Plate I was confirmed. Fig. 2 of Plate I is the Lauephotograph taken with the same specimen, by sending the X-ray beam in the direction parallel to the flat surface of the specimen and perpendicular to the direction of the flow of the metal. From this photograph, it became also clearer that the (211) plane is nearly parallel to the flat surface of the specimen and the [111] axis is parallel to the direction of the flow of the metal, and that the degrees of the deviation of the crystallographic orientations of the micro-crystals from the ideal orientation are just as already stated. Fig. 3 shows the

ideal orientation of the micro-crystals in a specimen compressed to such a high degree.

(II) The [211] axis is parallel to the direction of the flow of the metal, the [111] axis is nearly parallel to the direction of the longer side of the specimen, and consequently the (110) plane is nearly parallel to the flat surface of the specimen.

(a) of Fig. 4 represents the initial crystallographic orientation of a single crystal specimen whose thickness is 1.10 mm. in stereographic projection. AB is the direction of the longer side of the specimen and CD is the direction of the flow of the metal on compression. For slight compression in this case, the [211] axis, shown by a cross, becomes the axis of rotation of the micro-crystals, as stated in the report on the former investigation. But, as the compression was

Fig. 4

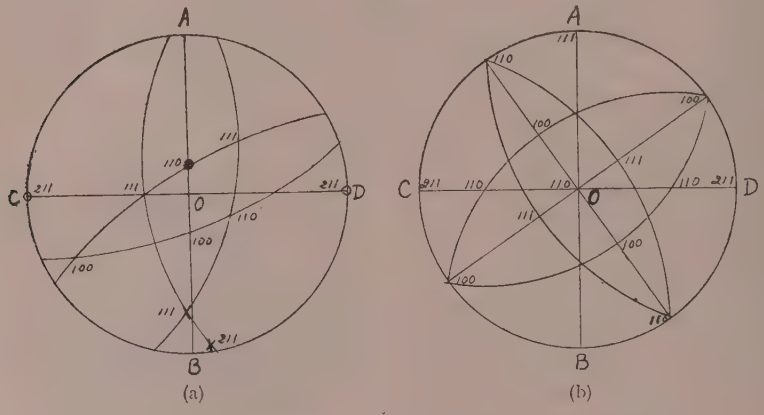

increased more and more, it was impossible for the [211] axis to continue to be the axis of rotation of the micro-crystals. Instead of the [211] axis, the [111] axis, shown also by a cross, gradually became nearly parallel to the direction of the longer side of the specimen and this axis became the axis of rotation of the micro-crystals for the compression to less than 20% of the initial thickness. Consequently the [110] axis, shown by a dot, approached gradually to the centre O, and the [211] axis, shown by a small circle, became nearly parallel to the direction of the flow of the metal. Fig. 3 of Plate I is a Laue-photograph taken with a specimen which was compressed to a thickness of 3% of the initial thickness, by sending the X-ray beam

normally to its flat surface. This photograph shows that the [111] axis is nearly parallel to the direction of the longer side of the specimen and the [211] axis is nearly parallel to the direction of the flow of the metal on compression. Thus the ideal orientation of the micro-crystals in a specimen which is compressed to such a high degree is just as shown by (b) of Fig. 4. Next, as in case (I), the writer calculated the deviation of the crystallographic orientation of the micro-crystals in the specimen from the ideal orientation by means of Fig. 3 of Plate I, and ascertained that the maximum deviation of the [211] axis, which was nearly in the direction of the flow of the metal, from the flat surface of the specimen was about $\pm 13^\circ$ and that the maximum deviation of the [111] axis, which was nearly in the direction parallel to the longer side of the specimen from the flat surface was $+21^\circ$ and -15°. This inequality of the deviation on the two sides of the flat surface seems to be due to the initial great inclination of the [111] axis to the flat surface of the specimen. Thus the (110) plane, which is nearly parallel to the flat surface, deviated by $\pm 13^\circ$ in the direction of the flow of the metal on compression, and by $+21^\circ$ and -15° in the direction parallel to the longer side of the specimen. As the deviation of the [211] axis is less than the deviation of the [111] axis, it seems to be natural to consider that the axis of the fibrous arrangement of the micro-crystals is the [211] axis which is nearly parallel to the direction of the flow of the metal for compression of such a high degree. The above-stated facts were also ascertained by the following consideration as was done in the case (I). The writer assumed the [211] axis to be the fibrous axis which is in the direction of the flow of the metal on compression, and the [111] axis the longer side of the specimen. Then, by taking into consideration the above-stated deviation of the crystallographic orientation of the micro-crystals from the ideal orientation, the diffraction diagram of the X-ray that might be expected to be impressed on a photographic plate by the K_α-line of molybdenum was calculated. Fig. 5 shows the diagram thus calculated and a fair agreement between this diagram and the photograph reproduced in Fig. 3 of Plate I was observed. Fig. 4 of Plate I is the Laue-photograph taken with the same specimen, by sending the X-ray beam parallel to the flat surface of the specimen and perpendicular to the direction of the flow of the metal. From this photograph, it became also clearer that the above stated consideration was correct. Fig. 6 shows the ideal orientation of the micro-crystals in such a compressed specimen.

Fig. 5

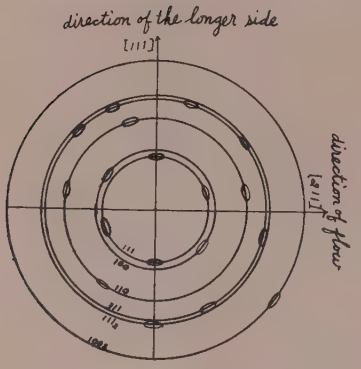

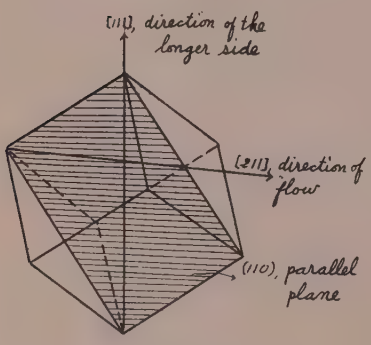

Fig. 6

(III) The [100] axis is parallel to the direction of the flow of the metal on compression, the [110] axis is nearly parallel to the direction of the longer side of the specimen, and consequently the (110) plane is nearly parallel to the flat surface of the specimen.

(a) of Fig. 7 shows the initial crystallographic orientation of a single crystal specimen whose thickness was 0.80mm. Here AB is the direction of the longer side of the specimen and CD is the direction of the flow of the metal on compression. As the process of compression proceeded the [110] axis shown by a cross, which was almost parallel to the direction of the longer side of the specimen, became the axis of the rotation of the micro-crystals; and the [110] axis shown by a dot approached to the centre O. Conse-

Fig. 7

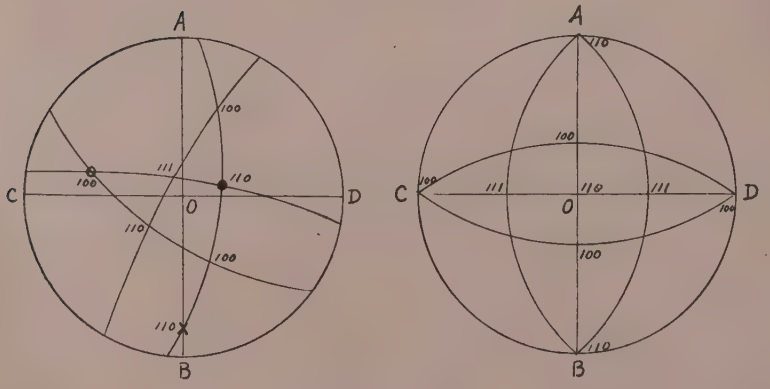

quently the [100] axis, shown by a small circle, became nearly parallel to the direction of the flow of the metal. Fig. 5 of Plate I shows the Laue-photograph taken with a specimen which was compressed to 8% of the initial thickness, by sending the X-ray beam normally to the flat surface. This photograph shows that the [110] axis is nearly parallel to the direction of the longer side of the specimen, and the [100] axis is nearly parallel to the direction of the flow of the metal on compression. Thus, the (110) plane must be nearly parallel to the flat surface of the specimen. The ideal crystallographic orientation of the micro-crystals of the specimen compressed to such a high degree is represented by (b) of Fig. 7. The deviation of the crystallographic orientation of the micro-crystals from the ideal orientation was estimated in the same way as in the former cases by means of Fig. 5 of Plate I. The maximum deviation of the [100] axis, which is nearly in the direction of the flow of the metal on compression, is about $\pm 13^\circ$ from the flat surface; and the maximum deviation of the [110] axis, which is nearly in the direction of the longer side of the specimen, is about $\pm 20^\circ$ from the flat surface. Thus the (110) plane, which is nearly parallel to the flat surface, deviates from the flat surface by $\pm 13^\circ$ in the direction of the flows of the metal on compression and by $\pm 20^\circ$ in the direction of the longer side of the specimen. As the deviation of the orientation of the micro-crystals in the direction of the [100] axis, which is nearly in the direction of the flow of the metal, is less than that in the direction of the longer side of the specimen, it seems to be natural to consider that the axis of the fibrous arrangement of the micro-crystals is the [100] axis which is parallel to the direction of the flow of the metal for a specimen compressed to such a high degree. Fig. 6 of Plate I is the Laue-photograph taken with the same specimen, by sending the X-ray beam parallel to the flat surface of the specimen and perpendicular to the direction of the flow of the metal. As the ideal orientation of the micro-crystals is just as shown by (b) of Fig. 7, the orientation of the micro-crystals in the following two cases is entirely the same with respect to the X-ray beam:—(1) when the X-ray beam is sent normally to the flat surface of the specimen, (2) when the X-ray beam is sent in the direction parallel to the flat surface and perpendicular to the direction of the flow of the metal. Consequently the photographs of Figs. 5 and 6 of Plate I which are impressed by the K_α-line of molybdenum must be similar to each other; and both of them must also be similar to the calculated diagram shown by Fig. 8 which is

drawn by taking into consideration the deviation of the micro-crystals from the ideal orientation. A fair agreement among these three figures supports the consideration mentioned before. Fig. 9 shows the ideal orientation of the micro-crystals in such a compressed specimen.

Fig. 8

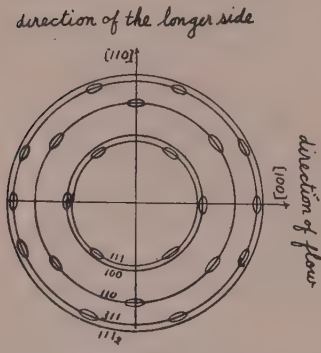

Fig. 9

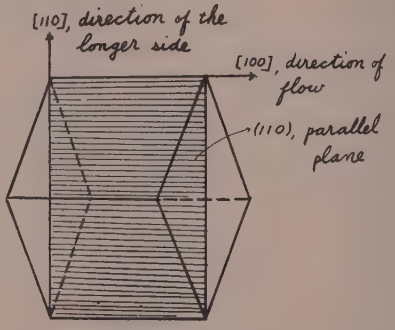

(IV) The [110] axis is parallel to the direction of the flow of the metal on compression, the [100] axis is nearly parallel to the direction of the longer side of the specimen, and consequently the (110) planes are nearly parallel to the flat surface of the specimen.

(a) of Fig. 10 shows the initial crystallographic orientation of a single crystal specimen whose thickness is 0.80 mm. The directions represented by AB and CD are respectively the same as stated in the

Fig. 10

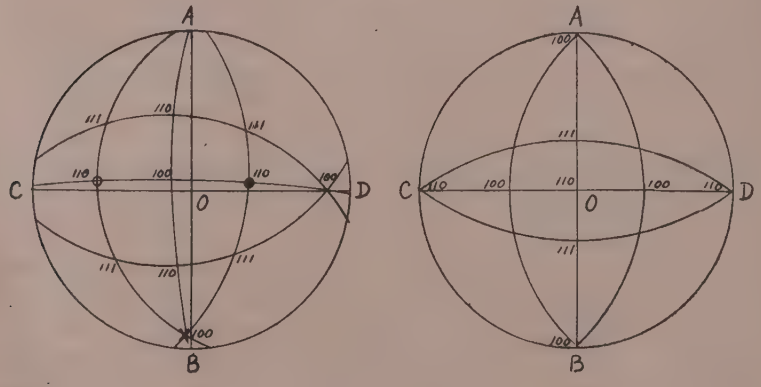

preceding sections. As the process of compression proceeded, the [100] axis shown by a cross became the axis of rotation of the micro-crystals and the [110] axis shown by a dot approached to the centre O, therefore the [110] axis shown by a small circle became nearly parallel to the direction of the flow of the metal gradually. Fig. 7 of Plate I is a Laue-photograph taken by sending the X-ray beam normally to the flat surface, with a specimen compressed to 10% of the initial thickness. From this photograph it is clear that the [100] axis is nearly parallel to the direction of the longer side, the [110] axis is nearly parallel to the direction of the flow of the metal, and consequently that the (110) plane is nearly parallel to the flat surface. Calculating from Fig. 7 of Plate I the direction of the crystallographic orientation of the micro-crystals from the ideal orientation, the writer found that the deviation of the [110] axis, which is nearly in the direction of the flow of the metal on compression was about $\pm 16^\circ$ from the flat surface, and the deviation of the [100] axis, which was nearly in the direction of the longer side of the specimen, was about $\pm 20^\circ$ from the flat surface. Thus it may be considered that the axis of the fibrous arrangement is the [110] axis which is parallel to the flow of the metal on compression. It follows, from the facts above stated, that the (110) plane which is parallel to the flat surface deviates from the flat surface by about $\pm 16^\circ$ in the direction of the flow of the metal and by about $\pm 20^\circ$ in the direction of the longer side of the specimen. As the ideal orientation of the micro-crystals is just as shown by (b) of Fig. 10 in this case, the crystallographic orientation of the micro-crystals in the specimen with respect to the X-ray beam is entirely similar in the following two cases:—(1) when the X-ray beam is sent normally to the flat surface, (2) when the X-ray beam is sent in the direction parallel to the flat surface and perpendicular to the longer side of the specimen. Fig. 8 of Plate I is a Laue-photograph taken by sending the X-ray beam parallel to the flat surface and perpendicular to the longer side of the specimen. By comparing Figs. 7 and 8 of Plate I we can detect a close resemblance between them. These two figures are also in fair agreement with Fig. 11 which is the diagram calculated from the consideration mentioned before. Fig. 12 shows the ideal orientation of the micro-crystals in this case.

The writer has mentioned in the preceding four sections that there are four different types in the manner of the fibrous arrangement of the micro-crystals when the rectangular single crystal plates of

Fig. 11

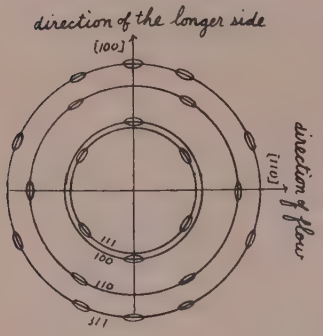

Fig. 12

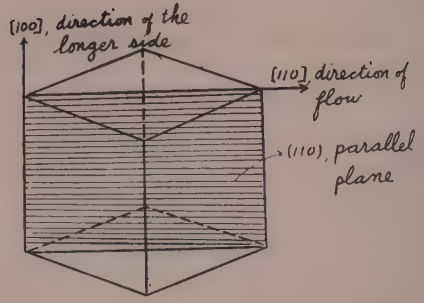

aluminium are compressed to less than 10% of the initial thickness. So far as the present experiment is concerned, whatever the initial crystallographic orientation may be, the final arrangement of the micro-crystals belongs to any one of the four types mentioned above, and the writer was not able to find out any other manner of arrangement of the micro-crystals. Of the four different types, the first two were observed to occur very much oftener than the last two. The final fibrous arrangements depend, of course, upon the initial crystallographic orientation of the single crystal specimen and the direction of the flow of the metal on compression. Thus, even though the rectangular specimens are prepared from the same single crystal plate, the manner of the fibrous arrangement ought not to be always the same, if the specimens are so prepared that the direction of the flow of the metal on compression is not the same from one specimen to the other. For example, let us mention the results which were obtained with specimens which were so prepared from the same single crystal plate that the direction of the flow of the metal on compression was different in different specimen. Fig. 13 shows the initial crystallographic orientation of a single crystal plate whose size was 4 cms. × 1.5 cms. × 0.8 mm. Four rectangular specimens were so prepared from the mother crystal that the directions of the longer side were parallel to the lines AB, CD, EF, and G11 respectively, the angle between any two successive lines being 30°.

(a) When the specimen whose longer side was parallel to the direction AB was compressed to 10% of the initial thickness, the fibrous arrangement of the micro-crystals was as follows:— the [111] axis shown by a cross on the line AB becomes nearly parallel to the

direction of the longer side, the [110] axis shown by a dot approaches to the centre O, and consequently the [211] axis shown by a small circle on the line GH becomes parallel to the direction of the flow of the metal on compression. This fibrous arrangement is the same as case (II) mentioned before. Fig. 1 of Plate II is a Laue-photograph taken by the normal incidence of the X-ray beam to the flat surface of the compressed specimen, and Fig. 2 of Plate II is one taken by sending the X-ray beam parallel to the flat surface and normal to the longer side of the specimen. These photographs show that the above stated facts are correct.

Fig. 13

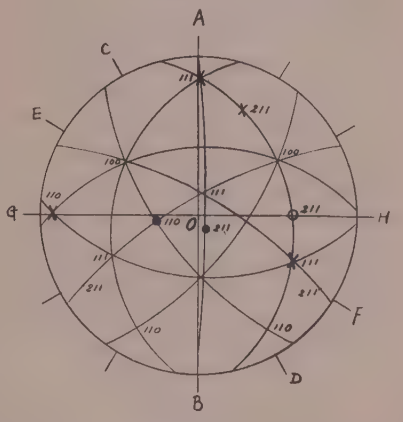

(b) As the writer has already given in case (III) details about the same specimen whose longer side is parallel to CD, the description of it is omitted here.

(c) When the specimen whose longer side was parallel to EF was compressed to the same high degree as before, the fibrous arrangement of the micro-crystals was as follows:— the [111] axis shown by a cross on EF becomes nearly parallel to the direction of the longer side, the [110] axis shown by a dot approaches to the centre O, and consequently the [211] axis shown by a cross becomes nearly parallel to the direction of flow of the metal. Such arrangement of the micro-crystal is the same as in case (II). Figs. 3 and 4 of Plate II are the Laue-photographs taken by the normal and the parallel incidence of the X-ray beam to the flat surface of the specimen respectively, and show that the above stated facts are correct.

(d) When the specimen whose longer side was parallel to GH was compressed to the same high degree as before, the fibrous arrangement of the micro-crystals became as follows:— the [110] axis shown by a cross on GH becomes nearly parallel to the direction of the longer side, the [211] axis shown by a dot approaches to the centre O, and consequently [111] axis shown by a cross on the line AB becomes parallel to the direction of the flow of the metal. This fibrous arrangement is just as in case (I). Figs. 5 and 6 of Plate II are

the Laue-photographs taken by the normal and the parallel incidence of the X-ray beam to the flat surface of the specimen respectively and show that the above stated facts are correct.

As reported in the former investigations, in the compressed circular plates, the manner of the fibrous arrangement of the micro-crystals was rather simple. In compressed rectangular plates it was seen to be different and not so simple as in the circular plates. But there seems not to exist any fundamental difference between the two cases and some complexity in the latter case seems to be due merely to the shape of the specimen. If the initial crystallographic orientation in a rectangular specimen is known, we can now easily find out the fibrous arrangement of the micro-crystals in a specimen compressed to such a high degree, by the aid of the crystallographic globe.

Let us suppose that the equatorial plane of the crystallographic globe is the flat surface of the specimen and a diameter which lies in this plane is the direction of the longer side of the specimen. Then the pole of the globe is the direction of the normal to the flat surface of the specimen. If a [111] axis on the hemispherical celluloid cap of the globe is made to coincide with the direction of the diameter, the number of the [110] axes which lie on the great circle, passing through the pole perpendicularly to the diameter, is six. The angle, which any two adjacent ones of these [110] axes subtends at the centre, is 60°. Consequently the angle between the pole and the [110] axis which is the nearest to the pole is less than 30°. Thus, for full compression, the direction of the [111] axis which is parallel to the longer side remains unchanged and the [110] axis which lies on the great circle and is the nearest to the pole approaches completely to the pole and the [211] axis becomes the direction of the flow of the metal. Therefore the ideal orientation of the micro-crystals becomes just as shown in Fig. 6. Next let us suppose that the [110] axis is parallel to the longer side of the specimen and this axis is made to coincide with the direction of a diameter lying on the equatorial plane of the crystallographic globe. The number of the [110] axes which lie on the great circle passing through the pole and perpendicularly to the diameter is only two in this case; and the angle which these two [110] axes subtend at the centre, is 180°. Moreover there are four [211] axes on the great circle. When the micro-crystals rotate around the [110] axis parallel to the longer side of the specimen, the one of the [110] and [211] axes which lies on the great circle and is nearest to the pole approaches to the pole on compression.

When one [211] axis approaches to the pole, the direction of the flow of the metal becomes the [111] axis, and the ideal orientation of the micro-crystals is just as shown in Fig. 3. If one [110] axis approaches to the pole, the [100] axis becomes parallel to the direction of the flow of the metal on compression, and the ideal orientation of the micro-crystals is just as shown in Fig. 9. Thus if the [110] axis is parallel to the longer side of the specimen, there may happen two different types of the fibrous arrangement caused by full compression. Even if the [111] or the [110] axis deviates initially more or less from the direction of the longer side, the final fibrous arrangement of the micro-crystals becomes any one of the above stated three types of the fibrous arrangement on full compression. When the [100] axis is parallel to the direction of the longer side, this axis becomes the axis of rotation of the micro-crystals and its direction remains unchanged during the whole process of compression. Now make one [100] axis on the hemispherical celluloid cap of the crystallographic globe coincide with a diameter in the equatorial plane of the crystallographic globe. Then the number of the [110] axes which lie on the great circle passing through the pole perpendicularly to the diameter, which is parallel to the longer side of the specimen, is four; and the angle which any two adjoining ones of these [110] axes subtend at the centre is 90. Thus, of these four [110] axes, the one which is nearest to the pole makes the angles less than 45° with the pole. Consequently, on compression, the [110] axis which is nearest to the pole as above stated approaches to the pole, making another [110] axis parallel to the direction of flow of the metal on compression. The ideal orientation of the micro-crystals in this case is as shown in Fig. 12.

It has already been stated that, of the four different types of arrangement of the micro-crystals, the first two are more frequent than the others. This seems to be easily explained, at least to some extent, by the possible number of the crystallographic axes present in the cubic crystal of aluminium as shown in Table I. Let us suppose that the frequency of occurrence of the four types is primarily influenced by the possible number of the crystallographic axes which are to be arranged parallel to the longer side of the specimen. Such numbers for respective types is given in the third column of Table I. This number is three in the fourth type, and it is the smallest compared with that of the other types. This is in agreement with the

Table I

Type	The axis parallel to the longer side of the specimen		The axis parallel to the direction of the flow of metal		The axis normal to the flat surface of the specimen	
	Axis	possible number	Axis	possible number	Axis	possible number
(1)	[110]	6	[111]	2	[211]	2
(2)	[111]	4	[211]	3	[110]	3
(3)	[110]	6	[100]	1	[110]	1
(4)	[100]	3	[110]	2	[110]	2

fact that the fourth type is not so frequent as the first two types. Next if we assume, as was considered above, that the crystallographic axes which are to be arranged parallel to the longer side of the specimen are primarily selected, then the crystallographic axes which are to be arranged parallel to the direction of the flow of metal by compression and those which are to be arranged parallel to the normal to the flat surface of the specimen must be those which are perpendicular to the crystallographic axes selected primarily as to be arranged parallel to the longer side of the specimen. The numbers given in the fifth and seventh column of the table are obtained in this way. In types (1) and (3), the crystallographic axes which are to be arranged in the direction parallel to the longer side of the specimen are the same; and consequently their possible numbers are equal too. However, the possible numbers of the axes which are to be arranged in the direction parallel to the surface normal of the flat surface of the specimen are not the same; they are 2 and 1 respectively. This is in good agreement with the fact that type (1) is more frequent than type (3).

Lastly let us consider the relation between the fibrous arrangements of the micro-crystals produced by compression and by rolling the aluminium plates. Prof. U. Yoshida was of opinion that the mechanism of compression and of rolling of metal might be essentially the same, if we regard the direction of the flow of the metal on com-

1. These Memoirs, **10**, 303 (1927)
2. Zs. f. Physik, **14**, 328 (1923)
3. Zs. f. Physik, **28**, 69 (1924)

pression as the direction of rolling. Investigations of the fibrous arrangement of the micro-crystals of aluminium caused by rolling have been carried out by S. Tanaka[1], Mark and Weissenberg[2], Weber[3] and others. S. Tanaka found three types of fibrous arrangement of the micro-crystals in rolled single-crystal plates. The first two types which occurred very often in the present investigation are similar to two of the three types found by S. Tanaka. Two Laue-photographs were taken by sending the X-ray beam normally to the flat surface of compressed and rolled polycrystalline aluminium foils respectively, which were reduced to 4% of the initial thickness in both cases. Figs. 7 and 8 of Plate II show respectively the photographs taken with the compressed and the rolled foils of polycrystalline aluminium foils. From these figures it was observed that the [211] axis was nearly parallel to the direction of the flow of the metal on compression or to the direction of rolling, the [110] axis was nearly parallel to the surface normal of the flat surface and the [111] was nearly perpendicular to the former two axes. Thus we see that, in polycrystalline plates, the fibrous arrangement of the micro-crystals produced by compression is similar to that of the micro-crystals produced by rolling, and that this arrangement belongs to the second type mentioned before. These facts seem to support the view that the mechanism of compression is essentially the same as that of rolling, as was suggested by Prof. U. Yoshida.

In conclusion, the writer wishes to express his sincere thanks to Prof. U. Yoshida for his kind guidance and suggestions.

Plate I

Fig. 1

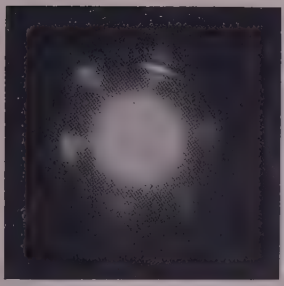

Fig. 2

Fig. 3

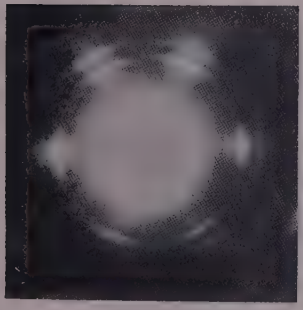

Fig. 4

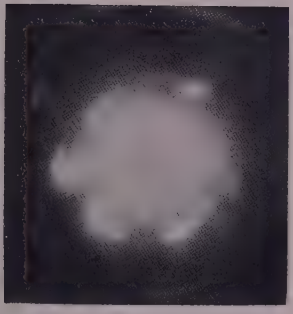

Fig. 5

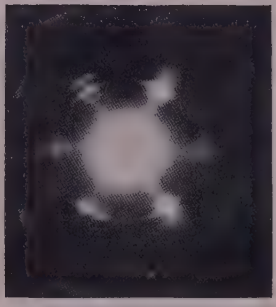

Fig. 6

Fig. 7

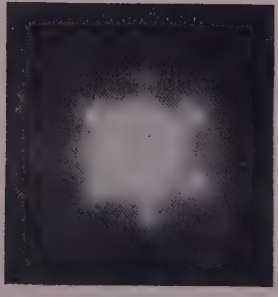

Fig. 8

Plate II

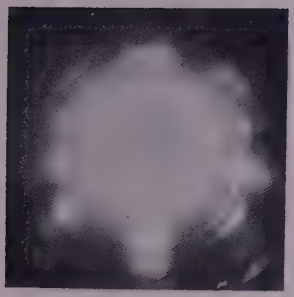

Fig. 1

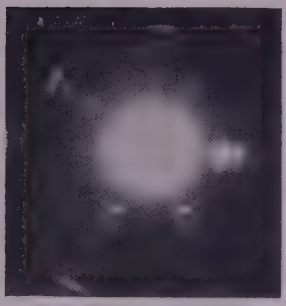

Fig. 2

Fig. 3

Fig. 4

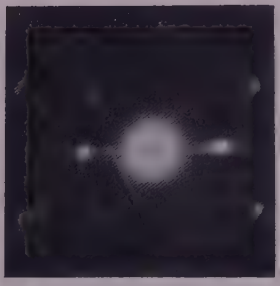

Fig. 5

Fig. 6

Fig. 7

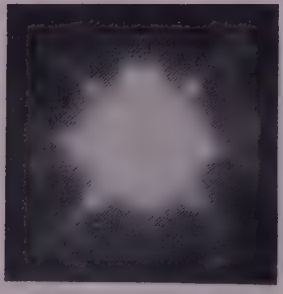

Fig. 8

X-Ray Diffraction Pattern of Native Cellulose

By

Usaburo Yoshida and **Noritomo Matsumoto**

(Received April 14, 1931)

Abstract

The form of the crystallographic unit cell of native cellulose was examined by X-rays. The diffraction spots A_3 and A_1 on the equatorial layer line were discarded as not being of K_α origin, the former spot being taken as of K_β origin and the latter as due to the critical absorption edge of bromine contained in the sensitive film of the photographic plate as silver bromide. The lattice form was taken to be tetragonal, having the edges $a=b=7.79$ A. U., and $c=10.26$ A. U.; and 4 $C_6H_{10}O_5$-groups are supposed to be contained in a unit cell.

The crystalline structure of cellulose is a subject which has been discussed already by many authors. The form of the crystallographic unit cell of native cellulose, as revealed by X-ray diffraction, is considered to be orthorhombic by Polanyi[1] and Herzog[2], and also to be an orthorhombic structure of different size by O. L. Sponsler[3]. A refinement of the orthorhombic structure suggested by Polanyi and Herzog, a monoclinic structure, which is only a little different from the orthorhombic one, was proposed by Mark and Meyer[4], and worked out thoroughly by Andress[5]. Many authors agree in saying that the identity period c, that is the length of the crystallographic axis of the unit cell of the crystallite in the direction parallel to the axis of the fibre of the native cellulose, is about 10.3 A. U., this having been

1. M. Polanyi: Naturwiss., **9**, 228 (1921)
2. R. O. Herzog: J. Physic. Chem., **30**, 457 (1926)
3. O. L. Sponsler: J. General Physiol., **9**, 677 (1926)
4. H. Mark and K. H. Meyer: Ber. D. Chem. Gesels., **61**, 593 (1928); Z. s. physik. Chem., **2**, 115 (1929)
5. K. R Andress: Z. s. physik. Chem., **136**, 279 (1928); and **2**, 380 (1929)

determined from the distribution on the photographic plate of the layer lines which are obtained by sending the monochromatic X-ray beam perpendicularly to the axis of the fibre. If the lengths of the two crystallographic axes of the unit cell which are both perpendicular to the c axis mentioned above, are represented by a and b, there is a great discrepancy in opinion among many authors as to the magnitudes of the a and b axes and the angle between these two axes. With regard to these points, the positions and the distribution of the diffraction spots belonging to the equatorial layer line on the photograph have the prime importance, and they have been examined very closely by many authors. According to O. L. Sponsler[1], K. R. Andress[2] and H. Mark and H. Meyer[3] the diffraction spot A_3, as it was designated by Herzog, is of K_β origin, and not due to the K_α line of the copper target they used. This point was also confirmed by the writers by filtering off as far as possible the K_β line of copper with a thin nickel foil, as is shown by the photograph reproduced in Fig. 1 of the annexed Plate, which was taken with native ramie fibre. Thus, as this spot has no bearing on the determination of the lattice form of native cellulose, it was omitted in the following.

When we use the X-rays coming from a copper target, the diffuse spots A_1 and A_2 overlap each other considerably as is illustrated in Fig. 2 of the annexed Plate, which was taken with native ramie fibre, so that it is usually difficult to measure their positions accurately. However, when the photograph is taken with the X-rays coming from an iron target, these two spots are separated clearly as shown in Fig. 3 of the annexed Plate. The results obtained with the photographs taken by using the X-rays coming from the copper and the iron target are tabulated in Table I. In this table, the values of $\sin\theta$ obtained with the copper and the iron target are given in the second and the third column respectively for the spots A_1, A_2, A_3 and A_4, where θ is the glancing angle of the X-rays to an atomic plane in the crystallite. For comparison, the values obtained by Herzog and Andress are tabulated in the fifth and the sixth column respectively. In the fourth column is given the ratio of the $\sin\theta$ obtained with the iron target to that obtained with the copper target. For the spots A_2, A_3 and A_4 this ratio is nearly equal to 1.26, which is the ratio of the wave-

1. loc. cit.
2. loc. cit.
3. loc. cit.

lengths of the K-radiations from iron and copper. But for the spot A_1 it is different, and takes the value of 0.951, which may be looked upon as unity within the limit of experimental errors. If we disregard the spot A_3 which is of K_β origin due to the same atomic plane as the spot A_4, then we may say clearly that the spots A_2 and A_4 are

Table I

Spot	With Cu Target, Sin θ_{Cu}	With Fe Target, Sin θ_{Fe}	$\frac{\text{Sin } \theta_{Fe}}{\text{Sin } \theta_{Cu}}$	Sin θ_{Cu} (Herzog)	Sin θ_{Cu} (Andress)
A_1	.123	.117	.951	.1294	.1297
A_2	.143	.175	1.22	.1451	.1436
A_3	.186	.230	1.24	.1791	——
A_4	.202	.255	1.26	.1981	.1979

$\lambda_{K\alpha}$ {Fe . . . . 1.934 A. U., Cu . . . . 1.54 A. U., $\frac{1.934}{1.54} = 1.256$

$\lambda_{K\beta}$ {Fe . . . . 1.753 A. U., Cu . . . . 1.389 A. U., $\frac{1.753}{1.389} = 1.263$

caused by the reflection of the K_α radiation from the two sets of atomic planes of the crystallite which have different spacings. In the case of the spot A_1, the circumstances are different, and its position on the photograph remains unaltered though the cellulose is illuminated with the X-rays coming from the iron and the copper target. This peculiarity of the spot A_1 suggests that it may be due to the sudden increase in the photographic sensitivity at the wave-length corresponding to the critical absorption edge of bromine, which is contained as silver bromide in the sensitive film of the photographic plate. As will be stated later, it seems to be quite reasonable to consider that the strongest spot A_1 is due to the second order reflection from the atomic planes having the spacing 7.79 A. U., between two successive atomic planes. As the crystallites are arranged fibrously, in our case, with a certain direction parallel to the atomic planes above mentioned as their common axis, the X-rays coming from the target are resolved and impressed on the photographic plate as their spectrum. The wave-length of the critical absorption edge of bromine is 0.918 A. U. Thus if we assume that the X-rays having this wave-length are subjected to the second order reflection from the atomic planes having eth

spacing value 7.79 A. U., then the value of $\sin\theta$ becomes 0.118, by Bragg's formula. This is in fair agreement with the value 0.117 obtained with the iron target, and also with 0.123 obtained with the copper target by the writers. The values observed by Herzog and Andress with a copper target deviate from the calculated one by about 10%. But the spot A_1 is very diffuse and overlaps the spot A_2 considerably with copper radiation, as was stated before. Moreover the spot A_1 is the nearest to the central spot caused by the direct X-ray beam. As these circumstances considerably hinder the accurate measurement of the position of this spot, a discrepancy of about 10% must be allowed for as the experimental error. The wave-length of the critical absorption edge of bromine corresponds to 13.5 K. V. s by the quantum relation. So if the X-ray tube is excited with a voltage higher than this critical value, we must always expect to get the impression of this critical absorption edge on the photograph, even if the K_β line is excluded by proper filtering. Figs. 2 and 3 in the annexed Plate were taken with copper and iron targets respectively, which were bombarded with about 25 K. V. cathode rays. In these figures we can detect that the weak continuous spectrum of X-rays runs from the spot A_1 to the very diffuse central spot.

If the consideration stated above, that the origin of the spot A_1 is the critical absorption edge of bromine, be correct, this spot must disappear when the X-ray tube is excited with a voltage lower than 13.5 K. V. s. This point was actually tested by exciting the tube, provided with a copper target, with a peak voltage of about 14 K.V.s. The presence of the A_1 spot and the continuous spectrum running from it to the central spot was scarcely perceptible in this case.

The appearance of the spot A_1, is very diffuse as was stated before. This is very different from the sharp image of the critical absorption edge in an ordinary spectrum obtained with a crystal of tolerable size. But if we consider that the crystals are very small in our case, as is revealed by the haziness of all the diffraction spots, it seems not to be altogether unnatural to regard the origin of the diffuse spot A_1 as the critical absorption edge of bromine.

Thus considering, the writers discarded the spot A_1, together with the spot A_3, in considering the lattice form of the native cellulose and it was found that the lattice form of the unit cell was very well expressed by a tetragonal form having the size :—

$$a=b=7.79 \text{ A. U., and } c=10.26 \text{ A. U.}$$

With this size of unit cell the quadratic equation becomes

$$\frac{4\sin^2\theta}{\lambda^2}=0.0165(p^2+q^2)+0.0095\,r^2,$$

where λ is the wave-length of the X-rays employed expressed by the unit A. U., and p, q, r are the indices of the atomic planes. The values of $\frac{4}{\lambda^2}\sin^2\theta$ calculated and observed by the writers, by Andress and by Herzog are tabulated in Table II. The agreement between the observed and the calculated values seems to be within the limit of experimental errors, excepting a few spots of weak intensity. For the spots of poor agreement the mark (?) is attached to the respective spots in the first column.

The spot A_6 is only observed by Andress. Though the observed value is somewhat larger than that calculated, it seems not to be quite unreasonable to ascribe this discrepancy to experimental error, because this spot is stated to be very weak by Andress.

The spot I_4 is very diffuse. Thus this spot is considered to be caused by the overlapping of the two spots due to the (311) and (321) planes.

The very weak spot II_6 is only observed by Herzog, and its origin is ascribed to the overlapping of the two spots due to the (312) and (322) planes.

The observed values tabulated in Table II, which were obtained by the writers, are the mean values measured on several photographs, which are taken with the K_α line of copper and iron. As an example, a photograph taken with the unfiltered K radiation of copper is reproduced in Fig. 4 of the annexed Plate, which was taken with native ramie fibre.

From the numbers given in Table II, the discrepancy between the observation and the calculation can not necessarily be said to be very small. But if we consider the circumstance that by the squaring of the observed values of $\sin\theta$, the percentage error in Table II is double that of the direct observation, a discrepancy of such extent as is seen in the table seems to be permissible as experimental error for the present case, where the diffraction spots come out pretty diffused on the photographic plate.

By assuming the form and the size of the unit cell of cellulose to be as stated before, the writers calculated the number of the $C_6H_{10}O_5$-groups contained in a unit cell. The volume of a unit cell is equal to

Table II

Spots	Indices	$\frac{4}{\lambda^2}\sin^2\theta$				Intensity
		calc.	observed by the writers	observed by Andress	observed by Herzog	
	100	0.0165				
A_2	110	0.0330	0.0338	0.0348	0.0356	str.
A_4	200	0.0660	0.0693	0.0660	0.0662	v. str.
	210	0.0825				
	220	0.1320				
A_5	300	0.1485		0.149		w.
	310	0.1650				
A_6(?)	320	0.2145		0.240		v. w.
A_7	400	0.2640	0.267	0.264	0.270	m.
	410	0.2805				
	330	0.2970				
	001	0.0095				
I_1	101	0.0260		0.0245	0.0293	w.
I_2	111	0.0425		0.0446		v. v. w.
	201	0.0755				
	211	0.0920				
	221	0.1415				
I_3	301	0.1580	0.156	0.149	0.149	m.
I_4(?)	311	0.1745	0.194	0.190	0.1936	w.
	321	0.2240				
II_1	002	0.0380		0.0384		w.
II_2	102	0.0545	0.0565	0.0540	0.0549	str.
	112	0.0710				
II_3	202	0.1040	0.111	0.106	0.1092	str.
II_4	212	0.1205	0.125	0.122	0.1210	str.
II_5	222	0.1700		0.176		v. v. w.
	302	0.1865				
II_6(?)	312	0.2030			0.2252	v. w.
	322	0.2525				
II_7	402	0.3020			0.284	v. w.
	332	0.3350				
	003	0.0855				
III_1	103	0.1020	0.103	0.100	0.1018	m.
III_2	113	0.1185	0.121	0.116	0.1163	m.
III_3	203	0.1515	0.154	0.145	0.1507	str.
III_4	213	0.1680	0.174	0.150		w.
	223	0.2175				
III_5	303	0.2340	0.230		0.225	w.
III_6	313	0.2505	0.252		0.2455	w.
IV_1	004	0.1520	0.155	0.151		str.
	104	0.1685				
IV_2	114	0.1850	0.190	0.184	0.186	w.
IV_3	204	0.2180	0.222	0.214	0.2185	str.
	214	0.2345				
IV_4	224	0.2840			0.2882	w.
IV_5	304	0.3005	0.295			w.
	005	0.2375				
V_1	105	0.2540	0.259			w.
	115	0.2705				
	205	0.3035				
V_2	215	0.3200	0.321			w.
	225	0.3695				
	305	0.3860				
VI_1	006	0.3420		0.340		m.

$$a^2 \cdot c = (7.79 \times 10^{-8})^2 \times 10.26 \times 10^{-8} = 624 \times 10^{-24} \text{ c.c..}$$

By taking the density of cellulose to be 1.59, after Andress[1], the mass of a unit cell becomes

$$1.59 \times 624 \times 10^{-24} = 9.92 \times 10^{-22} \text{ gms.}$$

As the mass of a $C_6H_{10}O_5$-group is equal to

$$\frac{162}{6.06 \times 10^{23}} = 2.675 \times 10^{-22} \text{ gms.,}$$

the number of $C_6H_{10}O_5$-groups contained in a unit cell becomes

$$\frac{9.92 \times 10^{-22}}{2.675 \times 10^{-22}} = 3.71.$$

This is not a whole number. But when we consider the circumstances that the accurate determination of the density of native cellulose is very difficult, and moreover that there is reason to take the net density of native cellulose somewhat higher than the value observed actually, then it seems to be quite legitimate to take the number of $C_6H_{10}O_5$-groups contained in a unit cell of native cellulose to be four.

In conclusion, the writers' sincere thanks are due to Prof. G. Kita of the laboratory of industrial chemistry in the Kyoto Imperial University for his kind advice.

1. K. R. Andress: Z. s. physik. Chem., **136**, 279 (1928)

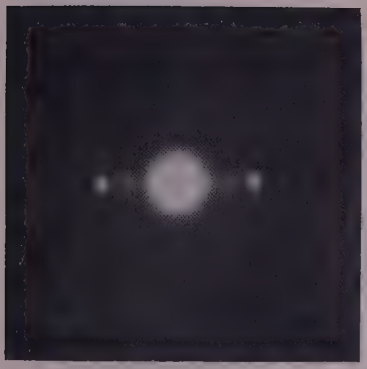

Fig. 1

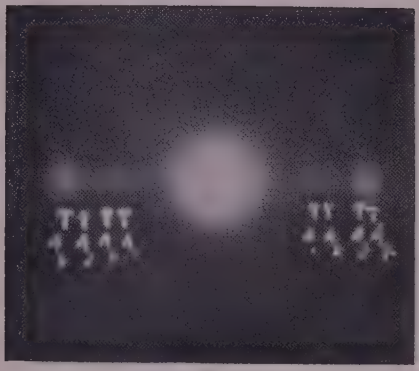

Fig. 2

Fig. 3

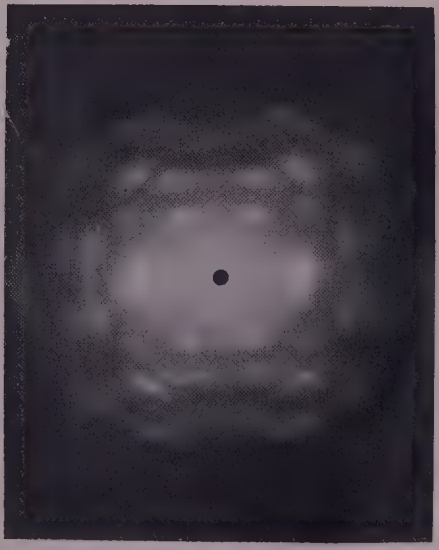

Fig. 4

Influence of Temperature upon the Diffusion Coefficient of Solid Metals

By

Chujiro Matano

(Received April 14, 1931)

Abstract

From the electrical resistance of foils composed of thin layers of two kinds of metals at various temperatures, the coefficients of diffusion D were determined successively by using the relation Dt=const. for the same kind of foils, where t is a time interval which is necessary to bring their resistance to some fixed value, the portion of the resistance due to the coefficient of temperature being removed. By means of this method it was confirmed that the relations $D=Ae^{-\frac{\alpha}{\theta}}$, and $D=A\theta e^{-\frac{\alpha}{\theta}}$, where A and α are constants and θ is the absolute temperature, show equally well the experimental results for the *Ag-Au* system and for the *Ni-Cu* system between 300°C (or 330°C) and 500°C.

Method of Successive Determination of Diffusion Coefficient

Theoretical part: If the samples are composed, as in the previous experiments[1], of many thin layers of two kinds of metals, and the electrical resistance of them is measured at various constant temperatures, then it will be found that the resistance will change as the time passes owing to the occurrence of the diffusion. Hence, if Fick's law holds good, the concentration c of one of the two metals will be given by

$$c=f\left(\frac{Dt}{d^2},\ \frac{a}{d},\ \frac{x}{d}\right),$$

1. S. Tanaka and C. Matano: These Memoirs **13**, 343 (1930); and **14**, 59 (1931)

where f is a certain known function[1] of three variables $\frac{Dt}{d^2}$, $\frac{a}{d}$ and $\frac{x}{d}$, D being the coefficient of diffusion, t the time, d the mean thickness of each layer, a half the thickness of the one metal, and x the one of the space coordinates which is perpendicular to the flat surface of the sample and has its origin in the middle of the one metal. The electrical conductivity k which is generally an unknown function of c will be put as

$$k=\varphi(c).$$

From these the conductance will be given by

$$K=\frac{Nl}{L}\int_0^d k\,dx=\frac{Nl}{L}\int_0^d \varphi(c)dx$$

$$=\frac{Nl}{L}\int_0^d \varphi\left\{f\left(\frac{Dt}{d^2},\ \frac{a}{d},\ \frac{x}{d}\right)\right\}dx=\frac{Ndl}{L}\psi\left(\frac{Dt}{d^2},\ \frac{a}{d}\right),$$

where N is the number of layers, l the breadth, and L the length of the sample. ψ is an unknown function of the variables $\frac{Dt}{d^2}$ and $\frac{a}{d}$.

In the previous paper S. Tanaka and the author[2] showed a method of determining the coefficient of diffusion by using the values of resistance near the saturation, but this method needs long time and, in practice, it is impossible except when the temperature is sufficiently high. To avoid this inconvenience, the author determined the coefficient D_1 at a temperature $T_1{}^0C$ in comparison with the known coefficient D_0 at a temperature $T_0(>T_1)^0C$, in the following way:—

Let us assume that two samples which have the same value of $\frac{a}{d}$, be used and heated at different temperatures T_1 and $T_0{}^0C$, and that the resistance of both is measured at $T_1(<T_0)^0C$. The sample at $T_0{}^0C$ is cooled to $T_1{}^0C$ only when the measurements are carried out. Then although the function φ is unknown, φ has the same form in both cases, and consequently ψ has the same form. So if we take $\frac{K_1L_1}{N_1l_1d_1}=\frac{K_0L_0}{N_0l_0d_0}$, or $\frac{R_1l_1d_1N_1}{L_1}=\frac{R_0l_0d_0N_0}{L_0}$ (where R is the resistance) and $\frac{a_1}{d_1}=\frac{a_0}{d_0}$, then corresponding to these, $\frac{D_1t_1}{d_1{}^2}=\frac{D_0t_0}{d_0{}^2}$, the suffix 1 here referring to the sample heated at $T_1{}^0C$ and suffix 0 referring to that at $T_0{}^0C$. Therefore

---

1. Riemann-Weber: Differentialgleichungen der Physik, II, p. 232
2. S. Tanaka and C. Matano: Phys. Math. Soc. Japan, Proc., **12**, 279 (1930)

$$D_1=\frac{t_0}{t_1}\left(\frac{d_1}{d_0}\right)^2 D_0,$$

and if d_1, d_0 and D_0 are known, then from the corresponding values of t_1 and t_0 we can determine D_1. And if we know the value of D_1 at $T_1{}^0C$, we can get the coefficient D_2 at $T_2(<T_1)^0C$ in the same way as above and we can get a series of values of coefficients at successively lower temperatures, without using the values of resistance near the saturation.

In such a simple case as when the same two samples are used,

$$\frac{N_1 l_1 d_1}{L_1}=\frac{N_0 l_0 d_0}{L_0}, \quad d_1=d_0 \quad \text{and} \quad a_1=a_0,$$

consequently

$$D_1=\frac{t_0}{t_1}D_0.$$

Experimental part: If we take the value of R far from its saturation, then in the first approximation we can take the temperature coefficient of resistance as that of pure component metals, and the results of our preceding paper[1] can be used at once without farther experiments, and the results are reproduced here again in Fig. 1a, 1b.

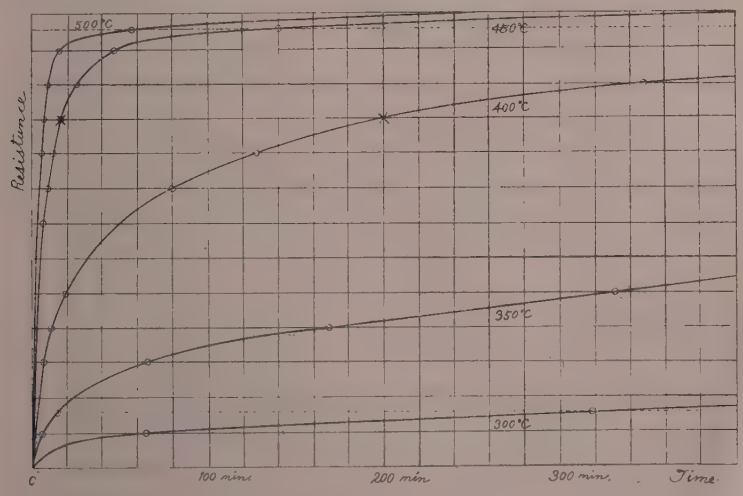

Fig. 1a Ni-Cu

1. S. Tanaka and C. Matano: These Memoirs, **14**, 59 (1931)

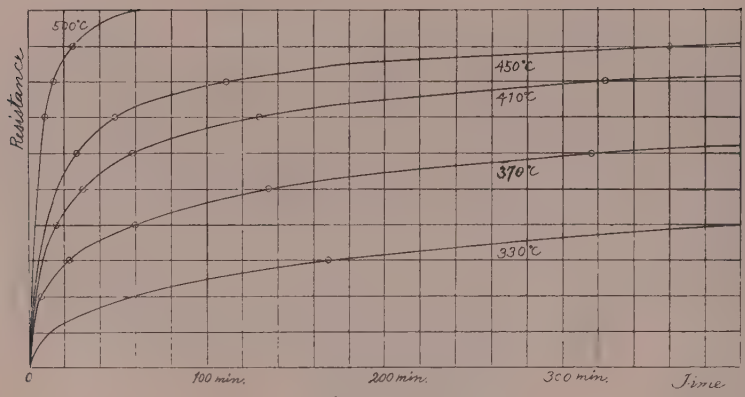

Fig. 1b Ag-Au

Here the portion of resistance due to the temperature coefficient is removed in each curve. The ordinates represent the resistance and the abscissae the time. Fig. 1a is for the *Ni-Cu* system and Fig. 1b is for the *Ag-Au* system.

For example, in Fig. 1a, let two corresponding points marked × on the curve at 450°*C* and on the curve at 400°*C* be taken, then graphically

$$\frac{D_{400}}{D_{450}} = \frac{17.0}{200} = 8.5 \times 10^{-2},$$

where D_{450} and D_{400} show the coefficients of diffusion at 450°*C* and

Table I

Material	Temperature *T*°*C*	Temperature θ°abs.	Ratio of Diffusion Coefficients at two succes. Temps.	Ratio of Diffusion Coefficients at *T*°*C* to 500°*C*	Diffusion Coefficient *D* cm.²/min.
Ni-Cu	500	773		1	0.7×10^{-12}
	450	723	3.7×10^{-1}	3.7×10^{-1}	2.6×10^{-13}
	400	673	9.3×10^{-2}	3.4×10^{-2}	2.4×10^{-14}
	350	623	7.2×10^{-2}	2.5×10^{-3}	1.8×10^{-15}
	300	573	5.4×10^{-2}	1.3×10^{-4}	0.9×10^{-13}
Ag-Au	500	773		1	0.8×10^{-12}
	450	723	1.5×10^{-1}	1.5×10^{-1}	1.2×10^{-13}
	410	683	3.8×10^{-1}	5.7×10^{-2}	4.6×10^{-14}
	370	643	2.2×10^{-1}	1.25×10^{-2}	1.0×10^{-14}
	330	603	1.4×10^{-1}	1.75×10^{-3}	1.4×10^{-15}

400°*C*. In the same way the other corresponding points marked o on the curves are taken and the values at each temperature are tabulated in Table I.

As the values[1] of D_0 at 500°*C*, 0.7×10^{-12} cm²./min. for the *Ni-Cu* system and 0.8×10^{-12} cm²./min. for the *Ag-Au* system are taken, then the coefficients of diffusion at lower temperatures can be obtained. They are shown in Table I in the fifth column.

Relations between Temperature and Diffusion Coefficient

J. Frenkel[2], from his theory of the thermal agitation in solid bodies, has shown that the absolute temperature θ is related to the coefficient of self-diffusion D in the following way,

$$D = Ae^{-\frac{\alpha}{\theta}}, \quad \cdots\cdots(1)$$

where A and α are constants independent of θ, and e the base of natural logarithms. After him, W. Braunbek[3], from his theory of electrolytic conduction in solid bodies, got the relation

$$D = A\theta e^{-\frac{\alpha}{\theta}}; \quad \cdots\cdots(2)$$

here also A, α and e are constants. Recently W. Jost[4] has confirmed by the chemical method that Frenkel's law (1) holds in the case of the *Ag-Au* system.

The author has tried to verify these laws for the *Ni-Cu* system and for the *Ag-Au* system.

Let D_0, D_1, ..., D_n be the coefficients of diffusion at θ_0, θ_1, ..., θ_n abs. and the times for determining these successively be t_0', t_1; t_1', t_2; .....; t_{n-1}', t_n; then

$$\frac{D_n}{D_0} = \frac{D_1}{D_0}\frac{D_2}{D_1}\cdots\cdots\frac{D_n}{D_{n-1}} = \frac{t_0'}{t_1}\frac{t_1'}{t_2}\cdots\cdots\frac{t_{n-1}'}{t_n}$$

$$\equiv \prod_{m=1}^{n}\frac{t_{m-1}'}{t_m},$$

and $\prod_{m=1}^{n}\frac{t_{m-1}'}{t_m}$ can be determined experimentally as shown in the

1. S. Tanaka and C. Matano, loc. cit.
2. J. Frenkel: Zs. f. Phys., **35**, 652 (1926)
3. W. Braunbek: Zs. f. Phys., **44**, 684 (1927)
4. W. Jost: Zs. f. phys. Chem., **9**, 73 (1930)

preceding section. (See Table I, 4th column). If we trace curves between

$$\log_{10}\left(\frac{D}{D_0}\right) \text{ and } \frac{1}{\theta}, \quad \text{or} \quad \log_{10}\left(\frac{D}{D_0}\right)-\log_{10}\theta \text{ and } \frac{1}{\theta},$$

then in both cases we get nearly straight lines as shown in Fig. 2 a, 2 b and Fig. 3 a, 3 b.

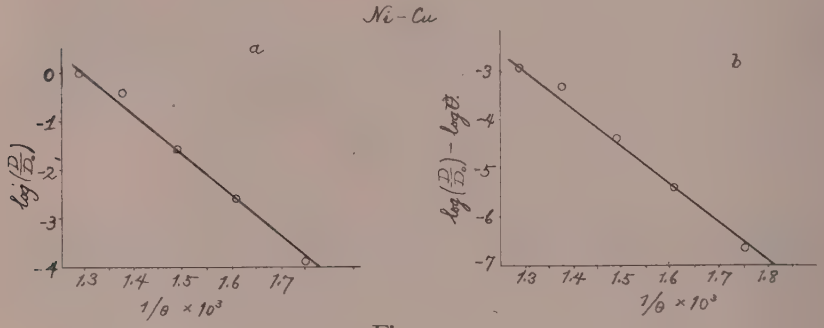

Fig. 2

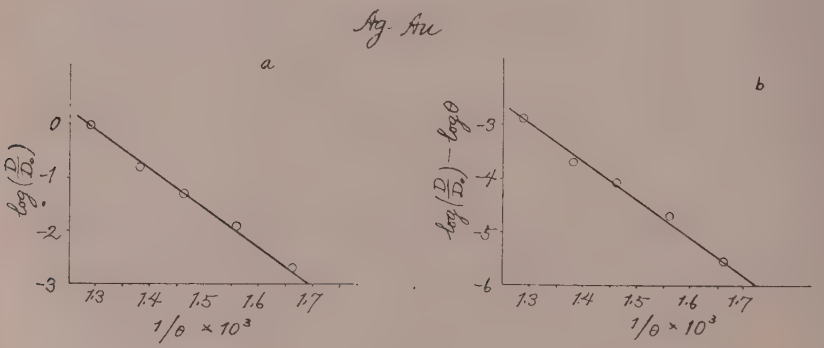

Fig. 3

So from the figures, for the *Ni-Cu* system

$$\log_{10}\left(\frac{D}{D_0}\right) = 10.50 - \frac{8.16 \times 10^3}{\theta},$$

or

$$\log_{10}\left(\frac{D}{D_0}\right) - \log_{10}\theta = 7.29 - \frac{7.19 \times 10^3}{\theta},$$

and for the *Ag-Au* system

$$\log_{10}\left(\frac{D}{D_0}\right)=9.70-\frac{7.51\times 10^3}{\theta},$$

or

$$\log_{10}\left(\frac{D}{D_0}\right)-\log_{10}\theta=6.44-\frac{7.24\times 10^3}{\theta}.$$

And if the relations in the forms

$$\log_{10}\left(\frac{D}{D_0}\right)=B-\frac{\alpha\log_{10}e}{\theta}, \quad \text{and}$$

$$\log_{10}\left(\frac{D}{D_0}\right)-\log_{10}\theta=B-\frac{\alpha\cdot\log_{10}e}{\theta}$$

exist, then

$$\frac{D_0}{e^{-\frac{\alpha}{\theta_0}}}=\frac{D}{e^{-\frac{\alpha}{\theta}}}=A, \quad \text{and} \quad \frac{D_0}{\theta_0 e^{-\frac{\alpha}{\theta_0}}}=\frac{D}{\theta e^{-\frac{\alpha}{\theta}}}=A,$$

where A, B and α are constants independent of θ, and the formulae (1) and (2) show the results of experiments equally well.

So far the value of D_0 has not been used, but if we want to get the value of A, the value of D_0 is needed. If we use the value of D_0 which is shown in the preceding section, the formulae (1) and (2) in their logarithmic forms are given by

$$\log_e D=-3.78-\frac{1.88\times 10^4}{\theta}, \quad \text{and}$$

$$\log_e D=-11.2+\log_e\theta-\frac{1.82\times 10^4}{\theta}$$

for the *Ni-Cu* system, and

$$\log_e D=-5.54-\frac{1.73\times 10^4}{\theta}, \quad \text{and}$$

$$\log_e D=-12.8+\log_e\theta-\frac{1.67\times 10^4}{\theta}$$

for the *Ag-Au* system. Comparing these results with W. Jost's, we can see at once though the values of D are somewhat different, in each case formula (1) is confirmed.

In conclusion the author wishes to express his sincere thanks to Prof. S. Tanaka for his kind advice on this work.

Physical Laboratory,
The Osaka University of Engineering,
March 1, 1931.

Vol. XIV, No. 3, Published May 30, 1931

Price - - - - Yen 1.20

These Memoirs are on Sale at

MARUZEN COMPANY, LTD.

TOKYO, OSAKA, KYOTO, NAGOYA, YOKOHAMA,
FUKUOKA & SENDAI

昭和六年五月二十五日印刷
昭和六年五月三十日發行

編纂兼發行者　京都帝國大學理學部

印刷者　須磨勘兵衞
京都市下京區北小路通新町西入

印刷所　內外出版印刷株式會社
京都市下京區西洞院七條南

賣捌所　丸善株式會社
東京、大阪、京都、名古屋、横濱、福岡、仙臺

CONTENTS

Mechanical Twins in White Tin and Zinc
By Kenzo Tanaka and Keiichi Kamio 79

Sur l'approximation successive et l'unicité de la solution de $\frac{dy}{dx}=f(x,y)$
Par Hirosi Okamura 85

The Arrangement of the Micro-Crystals in Compressed Single-Crystal-Plates of Aluminium. Part III.
By Yoshio Fukami 97

X-Ray Diffraction Pattern of Native Cellulose
By Usaburo Yoshida and Noritomo Matsumoto 115

Influence of Temperature upon the Diffusion Coefficient of Solid Metals 123
By Chujiro Matano . . . . . .